THE UNIVERSITY OF HULL

The Production of Trans-Lead Isotopes in the Intermediate Neutron Capture Process

being a Thesis submitted for the Degree of Master of Science (by Research) Physics in the University of Hull

by

George Harvey, B.Sc.

October 2022

Acknowledgements

I would like to give a massive thanks to Dr Richard Stancliffe, for helping me through a lot of the thesis, giving helpful notes and pushing me to continue when it felt like there was far too much work to do. He was also a very good therapist for keeping me sane through the entire process. I doubt I could have do it without him.

I would also like to thank everyone at the E.A.Milne centre. They made the thesis a fun experience when I was there. A special mention to Kate Womack who was excellent to bounce ideas off of throughout my research.

I would like to thank my friends who would help me relax after a days of working. They were a strong rock from the beginning and I could have done it without them. Special mention to Izzie Smith who pushed me when I was on the brink of giving up.

Finally, I would like to thank my family, Melanie, Simon and Elliot, who supported me with their love, care, food and constant badgering through it all. Also, a big thanks to Tilly the dog, who was an excellent rubber duck to help troubleshoot when things didn't go to plan.

Declaration of Originality

This thesis is submitted in partial fulfilment of the degree of MSc (by Research) Physics (Research) from the University of Hull. I declare that the work undertaken in this thesis is original and my own and was carried out under the supervision of Dr Marco Pignatari and Dr Brad Gibson. Where work, results, or ideas have been taken from other sources, those sources are explicitly referenced.

Candidates signature:

Date: 10/10/2022

Abstract

In the field of stellar nucleosynthesis, there were long believed to be two neutron capture processes responsible for heavy element production, the slow (s) and rapid (r) processes. However, recently a third process has been discovered that lies between the other two, dubbed the intermediate or i-process. So far, only the r-process has shown signs of trans-lead production, but the i-process could have the potential to do so as well. I investigate whether the i-process is able to produce trans-lead isotopes and whether these isotopes will remain after an extended period of time. I use a one-zone simulation, altering the temperature between runs, to see whether a post-AGB star with a large hydrogen intake is able to produce significant amounts of trans-lead isotopes. I also introduce the neutron-induced fission reactions for trans-lead isotopes to return some of the material to lighter, more stable isotopes. When the temperature gets higher, there is an increase in the production of trans-lead isotopes. With the introduction of the neutron-induced fission reactions, the unstable trans-lead isotopes at the upper end of the nuclide chart decay, creating pools of stability around thorium and uranium with significant production of these elements. The results of these runs are then compared to the star HE 0338-3945, which is an i-process enriched system with upper limits determined for both Th and U. The comparison showed that the production of Th would be exceeded for one of the temperatures and never for Uranium. It is possible for the i-process sites to produce trans-lead material under the right conditions, but more research into the area is required. A more developed method for the neutron-induced fission products could be made using a distribution curve of results. Further insight into other observable i-process sites could further develop our understanding of the i-process and trans-lead isotopes.

Contents

1. Introduction

At the beginning of the Universe, the Big Bang produced two elements in large abundance, hydrogen and helium, as well as small amounts of lithium and beryllium. Heavier elements were created as hydrogen and helium formed the first stars and nuclear fusion created elements up to iron. All other elements had to be made in a different way due to iron having the highest binding energy of any element, meaning atoms need energy to be put into the system to create elements heavier than iron. Almost all elements up to lead have at least one stable isotope, and these isotopes lie within the valley, or line, of stability. To create elements heavier than iron, neutron capture processes are typically needed. The s and r neutron capture processes were thought to be the only two that were required. However, there is a significant gap in neutron densities for the s and r process, and so a third neutron capture process was proposed, the i-process, that fills in the gap in between. The process is needed due to the presence of certain heavy elements found in stars, with abundances that do not follow the patterns of either the s or r process. The s and r processes behave very differently in terms of how the neutrons are produced and where they occur, but the s-process is very similar to the i-process in these aspects.

1.1 Neutron Capture Processes

In 1957, Burbidge, Burbidge, Fowler and Hoyle (Burbidge et al., 1957) (B^2FH) proposed a set of nuclear processes which explain elemental synthesis. B^2FH knew that not all stars show solar abundances due to their different enrichment histories. B^2FH were more looking at the distribution of the matter from observations and if it could be explained by capture processes. Given the limited knowledge in stellar physics at the time of publication, B^2FH mostly used their knowledge of nuclear physics to understand and explain key features in the solar abundance curve in figure 1.1. They proposed eight different elemental synthesis methods. Two of these processes, the s-process and the r-process, were described as using

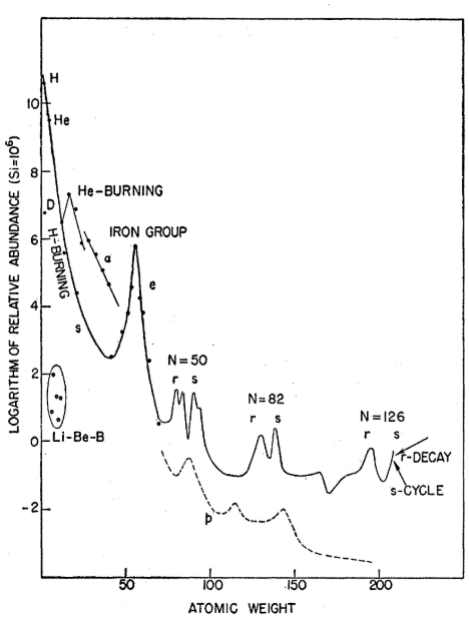

Figure 1.1: A graph showing the solar abundances of elements throughout the periodic table (Burbidge et al., 1957). There are peaks at hydrogen and iron, as hydrogen is the simplest element and iron is the most stable. The r and s peaks around N=50, N=82 and N=126 are due to the s and r process forming peaks around the magic numbers. The r-process peaks appear before the s-process peaks due the fact they reach each of the closed neutron shells with smaller proton numbers, giving the r-process lower mass numbers.

neutrons to create heavier elements. In figure 1.1, there is a large peak at hydrogen and helium, which we can expect as these elements make up a large portion of the baryonic mass in the Universe, and were the elements formed from the Big Bang. Later on we get a second peak at the iron group, which is formed by massive stars fusing atomic nuclei until it reaches iron, which is the heaviest element that releases energy when created by fusion. After the iron peak, there are three sets of two peaks with a peak in each set defined as s or r. These peaks are created by build up of s and r process material around the neutron magic numbers, which is when the neutron binding energy of isotopes is larger than the neutron binding energies of the surrounding isotopes.

A neutron capture process is one when an isotope captures a neutron, which would then become unstable, and such would decay back to the line of stability in the form of a β-decay. The s process, or slow neutron capture process, was first described by B^2FH. It is defined as having a neutron density of around 10^7 neutrons/cm^3 (Busso et al., 1999). As such, the time between the neutron captures is a long time, so β- decays occur more often

than a second neuron capture. Therefore, during the s-process, the nucleus will stay close to the line of stability (Busso et al., 1999). The production of neutrons primarily comes from neutron production around the CNO area. Neutrons occur when a ^{12}C nucleus reacts with a ^{1}H nucleus, resulting in a ^{13}C isotope. From here, the ^{13}C isotope reacts with a ^{4}He nucleus, which produces an ^{16}O atom and a neutron. An example of the s-process can be found in figure 1.2, where we see a zirconium nucleus capture neutrons and go through the s-process. When the nucleus first leaves the line of stability, it still captures a neutron at ^{93}Zr because the half-life of this isotope is 1.6×10^{6} yrs. However, when we get to ^{95}Zr, the half-life is short enough, only 64 days, that it will decay and continue to decay until the nucleus gets back to the line of stability at ^{95}Mo. Once the s-process ends, the material produced will peak at distinct neutron numbers, called neutron magic numbers. These numbers are 50, 82, and 126, where the neutrons in the nucleus are the most stable, and thus are less likely to capture anymore neutrons. The reason behind this stability is similar to the idea of electron shells, with full neutron shells being more stable. The isotopes for these magic neutron numbers are strontium, barium and lead (Hampel, 2015). These peaks can be seen in figure 1.1. The s-process does not go beyond lead as the neutron density is not large enough and there are no more stable isotopes, so lead is the largest isotope in the s-process. This is important as other processes may be able to create these unstable isotopes and will be discussed later on in the thesis.

The r-process, or rapid neutron capture process, is defined as having a neutron density of around 10^{20} neutrons/cm^3. This means that, unlike the s-process, a nucleus can go through multiple neutron captures before it begins to decay, and only decays when the half-life is significantly small, hence the reason it is called rapid. An example of this multiple capture process can be seen in figure 1.2, where we see the zirconium, which has reached ^{95}Zr, but continues to capture neutrons instead of decaying, going to ^{98}Zr and beyond. Because of this, the r-process tends to move material much further away from the line of stability. Once the r-process ends, and the neutron density has fallen, the material returns to the line of stability, but will create subtle broad peaks of material before the neutron magic numbers, as see in figure 1.1. The r-process can produce isotopes larger than lead, due to the neutron density,

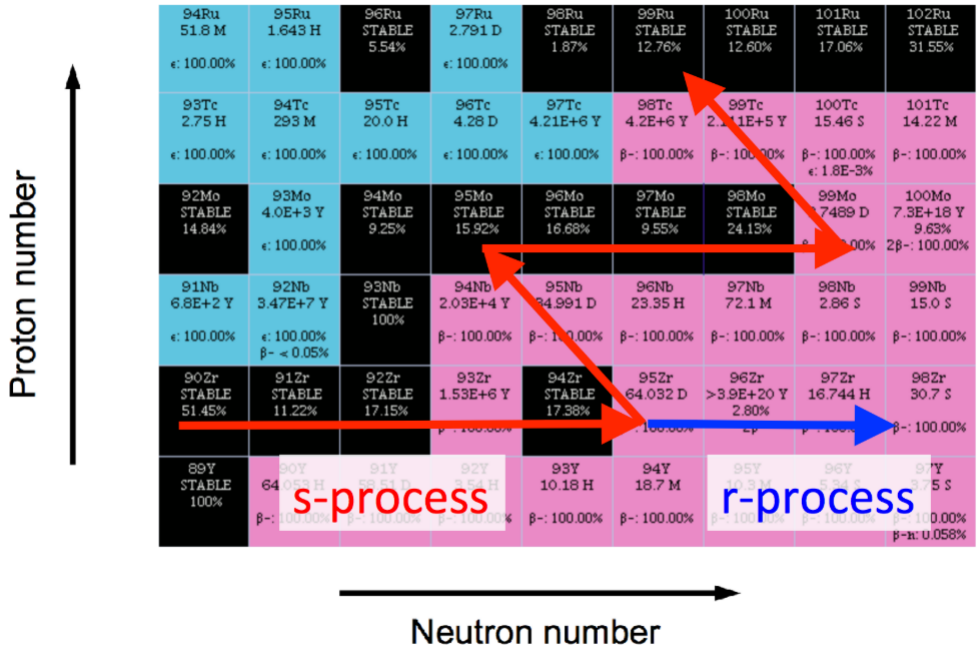

Figure 1.2: A small section of the nuclide chart (Hampel, 2015) showing the s-process (red arrows) and the r-process (blue arrow). Stable isotopes can be found in black. The lines show an example of neutron capture and beta- decay. The s-process stays close to the line of stability whilst the r-process strays further out and therefore can have broader peaks when it returns to the line of stability.

unlike the s-process.

The intermediate neutron capture process was first introduced by Cowan & Rose (1977). In their models, they calculate a neutron mass fraction of up to 10^{-10}, which when converted into a neutron density, is roughly 10^{17}cm^{-3}, a value outside of the boundaries of the s and r process presented in Blake & Schramm (1975) and Blake & Schramm (1976). There was also a much larger neutron flux in Cowan and Rose's models ($10^{23} - 10^{25}\text{cm}^{-2}\text{s}^{-1}$) compared to the s-process models of Blake & Schramm (1975) ($10^{15} - 10^{16}\text{cm}^{-2}\text{s}^{-1}$). Thus they determined a third neutron capture process called the intermediate capture process. The intermediate neutron capture process, or i-process, stands as the middle ground between the s and r processes, as it has a neutron density of roughly 10^{15} neutrons/cm^3. As said previously, it behaves similarly to the s-process in that it occurs in similar places in the galaxy and produces the neutrons in a similar way. The i-process occurs in low metallicity stars that pass through the AGB phase of their life-cycle, known as post-AGB stars. AGB and post-AGB stars have

already been identified as neutron production sites and a site for the s-process. The low metallicity refers to the low abundance of iron compared to of that in the Sun. The i-process can also occur within rapidly accreting white dwarfs (RAWDs), when a white dwarf accretes material from a larger companion star which is earlier in its life-cycle. Evidence for the i-process can be found in several locations in the universe. The first location is with Carbon Enhanced Metal Poor stars, or CEMP stars. CEMP stars are formed from the remnants of dying stars, and as such will have elements from those dying stars found within them. For this reason, it is possible to find CEMP stars which contain s-process material (CEMP-s stars), r-process material (CEMP-r stars) and i-process material (CEMP-r/s or CEMP-i stars) (Hampel et al., 2019) (Hampel, 2015) (Dardelet et al., 2018). More details about the CEMP stars are discussed at the end of the next section. Using spectroscopy, we can determine if a star falls within the limit of a CEMP-r/s star, which requires a [Ba/Eu] between 0 and +0.5. One of the first observable evidence for the i-process was from (Asplund et al., 1999), and the discovery of the born-again star Sakurai's object. This was further surmounted by (Herwig et al., 2011), also known as the Victoria group, who proved this using stellar models of Sakurai's object. The Victoria group have also worked on investigating the potential sites where the i-process can be found, such as RAWDs (Denissenkov et al., 2017) (Denissenkov et al., 2019) (Côté et al., 2018), and the Victoria group as a whole have made great progress on the i-process. Another key to understanding of the i-process is the work done by Hampel, especially her papers Hampel (2015), Hampel et al. (2016) and Hampel et al. (2019). Hampel (2015) develops the link between metal poor AGB stars, a production site for the i-process, and CEMP-r/s stars. CEMP-r/s stars were thought to be a mixture of the s-process and r-process abundance patterns, but could be explained better using the i-process as a single abundance pattern. Hampel et al. (2016) further develops the understanding by linking several CEMP-r/s stars with the abundance patterns from the i-process and proposing changing the name to CEMP-i star. Hampel et al. (2019) goes on to discuss the lack of lead in Magellanic s-process rich post-AGB stars, an element which should be relatively abundant, and a higher than average heavy element abundance in CEMP-s stars. Both of these are explained using the i-process nucleosynthesis as opposed to the s-process. Choplin et al. (2021) determines

that low-mass, low-metallicity AGB stars are able to produce i-process levels of neutrons and i-process elements during the early stages of the AGB phase. Dardelet et al. (2018) works on the CEMP-r/s stars and the relation between them and the i-process.

1.2 Origins of the i-process

It is important to understand where the i-process can occur within the universe. These sites include: AGB and post-AGB stars, very late thermal pulses in post-AGB stars, super AGBs, RAWDs and massive, fast rotating, metal-poor stars. AGB and post-AGB stars are those that are either still undergoing their asymptotic giant branch phase or have just past that stage in their evolution. They contain a large amount of hydrogen, helium and carbon. These stars undergo helium flashes that produce i-process materials by mixing the hydrogen into the intershell medium. Very late thermal pulses in post AGB stars occur when a star is progressing along the white dwarf track, on its way to become a white dwarf. When the star is close to being a white dwarf, the star might re-ignite with a helium flash that changes the star into a 'born-again' giant star. These stars are short lived but produce i-process material in the same way as AGB and post-AGB stars. Super AGB stars are AGB stars that have undergone carbon burning and now have an oxygen-neon electron degenerate core (Jones et al., 2016). They could have a similar method of producing neutrons to AGB stars but it is not confirmed yet. Rapidly accreting white dwarfs are white dwarfs in a binary star system that are donated material from the companion star which then allows the white dwarf to produce neutron capture materials, including i-process materials. Massive low-metallicty stars are those that were formed from the direct descendants of the first stars, where the only elements available were hydrogen and helium, and the low-metallicity stars have similar properties. Clarkson et al. (2018) describes such stars as following an i-process abundance distribution similar to their models.

Cowan & Rose (1977) discussed the production of neutrons within evolved red giant stars, these stars would undergo helium flashes and would produce i-process levels of neutrons. Such events occur within Asymptotic Giant Branch stars (AGB) or Post-Asymptotic Giant Branch stars (Post-AGB). These stars have undergone their main sequence phase, burning

their hydrogen and helium. If the helium shell becomes exhausted, but the hydrogen shell is still burning, the star is said to be thermally pulsing. The hydrogen shell continues to feed the helium shell until it can reignite in a helium flash. The AGB and Post-AGB structure is a carbon-oxygen core with a helium shell surrounding it, and a smaller hydrogen shell surrounding that. Between these two shells is a convective intershell where the hydrogen is brought down from the hydrogen shell by convective currents and mixes with the helium from the helium shell. Within the helium shell there will be carbon-12 that has been made and that will fuse with the hydrogen to create carbon-13. Carbon-13 is the start of the CNO cycle which produces neutrons, meaning there is a neutron production within AGB and Post-AGB stars. Malaney (1986) showed that the ingestion of hydrogen controls the production of neutrons, and this ingestion is key to the neutron densities needed for the i-process. Cowan & Rose (1977) found neutron number densities of $10^{15} - 10^{17}\text{cm}^{-3}$, which signifies the presence of the i-process. The i-process in AGB and Post-AGB stars was also proposed by Choplin et al. (2021), specifically within low mass, low metallicity AGB stars.

After a stellar body undergoes the AGB and Post-AGB phases, the star will travel along the white dwarf cooling track. During this track, a helium shell flash can occur. When a flash occurs close to the end of the track, the star will be classed as a 'born-again' giant star, as the stellar body reignites with a Very Late Thermal Pulse (VLTP), before returning to the white dwarf cooling track. Occurrences of this type of star are rare in the known universe. The probability for their occurrence is roughly 10% of all low and intermediate mass stars going through the planetary nebula phase (Asplund et al., 1999). However, these stars only have a short life-span, typically 100-1000 years, depending on the stellar envelope mass (Asplund et al., 1999). This is the reason why so few of these objects are found in the observable universe. One such 'born-again' star is called Sakurai's Object. Named after the amateur astronomer Yukio Sakurai, this stellar body has undergone a very late thermal pulse and, in observations, appears as a red giant. Sakurai's object is stated to have gone through hydrogen ingestion from the hydrogen-rich envelope of the star, which was caused by a helium flash (Asplund et al., 1999). This ingestion produces a large amount of ^{13}C, which in turn produces neutrons because of the presence of helium. This is stated to produce s-process material, a

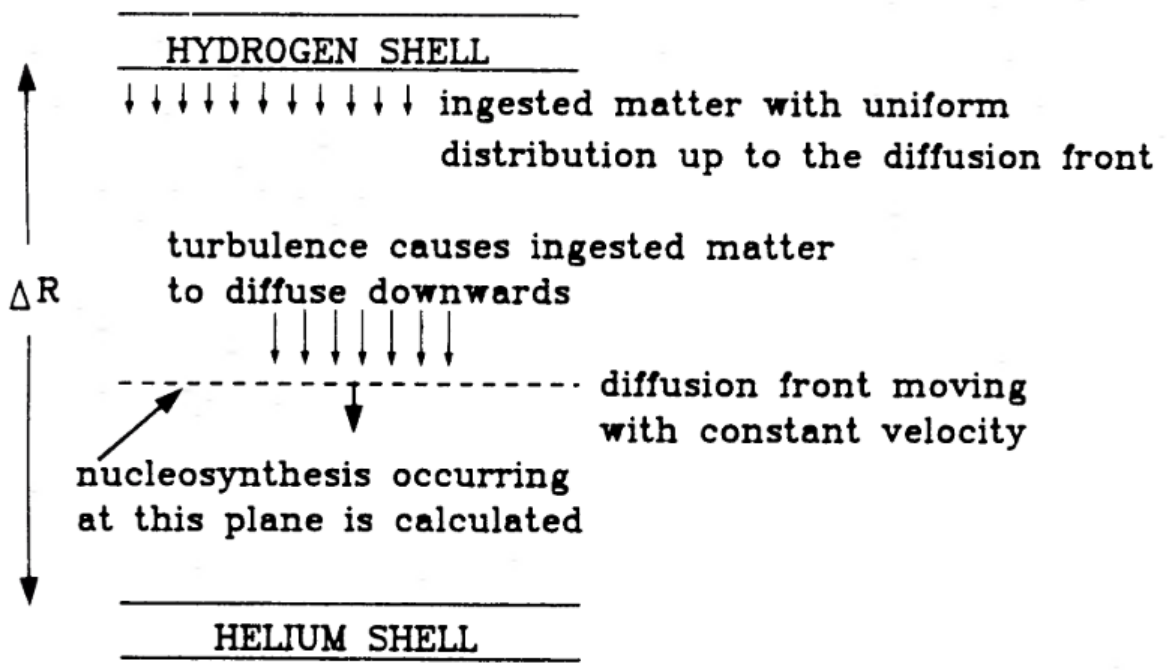

Figure 1.3: A description of the intershell medium from Malaney (1986). This figure shows the hydrogen in the hydrogen shell being brought further into the star by convective currents, which mixes with the helium and carbon from the helium shell. This is the primary production method of neutrons in AGB and Post-AGB stars and key to the neutron capture processes.

fact that matches theoretical expectations of Sakurai's object.

Another place where the i-process can occur is within Rapidly Accreting White Dwarf stars (RAWDs). These stars are carbon-oxygen white dwarf stars that accumulate mass from a companion star. They are formed when a star found within a binary system comes to the end of its life and becomes a CO white dwarf, and is then fed material from the companion star. The companion star will enter the red giant stage of its life-cycle, causing the companion stars outer layers to spread out from the core and enter the gravitational pull of the white dwarf. (Cassisi et al., 1998) first proposed that a carbon-oxygen white dwarf could accrete enough material to produce a helium flash. This was further developed by (Denissenkov et al., 2017), who investigated the mass retention of the RAWDs and proposed that the material produced fell in line with the production of the i-process. The area in which material will stay within the pull of both stars in the binary system is called the Roche Lobe. If the material exits the Roche Lobe from a direction away from its companion star, the material will be ejected into space. However, if the material travels from the red giant towards the white dwarf, the material is captured by the gravitational pull of the white dwarf. This matter is accreted into the white dwarf. If the material is too slow to transfer between stars, the material will not ignite, but instead will cause thermal pulses and the white dwarf will grow until a nova event. If the material transfers too fast, the accreted hydrogen will expand creating a red-giant envelope, and will also not produce neutron capture material. The necessary mass accretion rate for a rapidly accreting white dwarf is approximately $10^{-7} M \odot \mathrm{yr}^{-1}$ (Côté et al., 2018). Once the white dwarf reaches the Chandrasekhar mass (1.44M⊙), the star will explode as a type 1a supernova. This signifies the ignition of carbon fusion and expels the outer layers of the star, releasing any neutron capture material that was locked in outer layers of the white dwarf. Another way the i-process material can escape from the white dwarf is via super-Eddington-luminosity winds, where the star exceeds the Eddington luminosity and a radiation driven stellar wind expels the material.

One way to detect the presence of i-process materials is within carbon enhanced, metal poor stars (CEMP stars). These are stars that have a high level of carbon and a low level of metals compared to the Sun, with metals referring to any elements other than hydrogen

and helium. CEMP stars were initially discovered long ago. However, very metal poor stars became of greater importance when looking for the earliest formed stars. The stars found often had high amounts of carbon and low levels of iron due to the lack of metals and other heavy elements around the time of their formation, leading to a CEMP star. The first CEMP stars found were CEMP-no stars, although not referred as such, which followed the standard pattern of a CEMP star, which is defined as having a [C/Fe] $\geq$ +1, and a [Fe/H] $\leq$ -1. However, it was also discovered that some stars have an abundance of s-process material present. These CEMP-s stars were found within binary star systems, with an AGB companion star. AGB stars can produce s-process material, and these stars will deposit that material into their companion CEMP star. A similar process works for the CEMP-i stars. Initially, a CEMP-r/s was thought be a CEMP star that formed within an r-process rich nebula with an AGB companion, to have a mix of both s-process and r-process material as stated in (Bisterzo et al., 2012). However, CEMP-r/s were eventually determined to be found within a binary star system with an AGB star that produces i-process materials, and so are now referred to as CEMP-i stars. These CEMP stars can contain matter produced from neutron capture process sites and are therefore categorised by the amount of barium and europium the star has, as these relate to the s and r process respectively. CEMP-s stars contain s-process materials and can be identified by having a [Ba/Fe] $\geq$ +1 and a [Ba/Eu] $\geq$ +0.5. CEMP-r stars have a [Eu/Fe] $\geq$ +1 and a [Ba/Eu] $\leq$ 0. CEMP-r/s stars, or CEMP-i stars, contain i-process material and have a [Ba/Eu] between 0 and +0.5. Finally, CEMP-no stars have a [Ba/Fe] $\leq$ 0. CEMP-i stars are vital to the study of the i-process as they are one of the few places where the i-process has played a definitive role.

1.3 Trans-lead Isotopes

We already know that stars can produce elements up to and including iron via nuclear fusion, and that the neutron capture process can produce elements up to and including lead. We also know that the r-process can produce trans-lead elements which are not stable. Trans-lead isotopes are more commonly formed from neutron star mergers, where the high density of neutrons produce elements high up the nuclide chart. These isotopes will decay, first by β-

decay to a more stable isotope, and then back down the nuclide chart via alpha or nuclear fission decay, until they return to an isotope that is stable. There are four important isotopes in the trans-lead region that have a very long half-life and are classed as quasi-stable isotopes. These quasi-stable isotopes have long half-lives over 10^6 years, so they are present on Earth for a long time after being formed. These isotopes are ^{232}Th, ^{234}U, ^{235}U and ^{238}U. This means that they remain well past the rest of the trans-lead isotopes have decayed or undergone nuclear fission. These isotopes will be our way of detecting the presence of trans-lead isotopes within the production of a star. As we can see in Gull et al. (2018), we detect thorium within the star J0949-1617, which indicates the production of trans-lead isotopes. They determine from the spectra that the star must have both s and r process materials, which gives a good indication that the production could come from the i-process. In this thesis, I will be looking at the four quasi-stable isotopes, as these are key indicators for the creation of trans-lead elements.

The s-process is unable to create any trans-lead isotopes due to the lack of neutrons needed to move past lead. Because isotopes up to lead are near the line of stability, when they decay they will return to stability. This is the case for most of the s-process material. However, if any material makes it past lead, the material quickly decays back to stability via β- decays and α decays. In the case of the r-process, the neutron number is enough to surpass the barrier around lead and the r-process is able to produce trans-lead. The i-process has the possibility to produce isotopes past lead as the i-process has a larger neutron count than the s-process. So far, there is little, if any, work on the effect that the intermediate neutron capture process has on the trans-lead isotopes, and the literature for the i-process focuses on the isotopes leading up to lead.

The n-capture cross sections of isotopes are an important factor in the production of all isotopes, including trans-lead isotopes. The reaction rates determine how quickly isotopes capture or decay. One of these reactions could be neutron induced fission, (n,f), when neutrons (n) interact with unstable isotopes and fission (f) the material. This rate is especially important for the trans-lead isotopes, as these are the ones that are unstable because of the amount of total nucleons, and not because of an over abundance of either protons or neutrons. There is also the (n,g) rates, which is the rate at which neutrons (n) are captured by an isotope, and release

Figure 1.4: An extract of the nuclide chart from NuDat 3[1] containing a few trans-lead isotopes. Each square represents an isotope. Within each square we see the name of the isotope involved, the half-life of the isotope and the reactions that the isotope will go through during the decay. The percentage next to the types of reactions indicate that chance of that reaction occurring to a single atom of the corresponding isotope. If the isotope is stable or quasi-stable, then a percentage under the name will indicate the amount of that isotope found in the universe.

gamma particles (g). This is an important rate for all neutron capture processes, including the i-process. The (n,g) rates are what determine the likelihood of an isotope capturing a neutron and therefore the further away the isotope will travel from the line of stability. Another reaction rate is the rate of decay via the release of electrons. This is a reaction caused by the capture of neutrons and the unstable isotope that is formed as a result. When an unstable isotopes undergoes electron decay, or β- decay, the isotope will begin to return to the line of stability. This is primarily important for isotopes smaller than lead, as these are the areas that have a line of stability to return to. Past lead, β- decay can still happen, but other, more impactful reactions will occur.

An in-depth look into the production of trans-lead isotopes by the intermediate neutron capture process is necessary for a complete understanding of the i-process. As of now, the most detailed look at this section of the nuclide chart has been done by Choplin et al. (2022), a letter looking into the synthesis of thorium and uranium in AGB stars. Other descriptions of the i-process, such as that from Hampel (2015) and Denissenkov et al. (2019) fail to include the elements larger than polonium. It is important for a full understanding of the i-process to explore further up the nuclide chart, to see thorium, uranium and the isotopes that decay to become the quasi-stable isotopes within elements. To that end, extending the nuclide chart up to californium will be key to understanding the interaction between the i-process and the trans-lead isotopes. Adding reactions to include neutron induced fission will also extend the work done by Choplin et al. (2022) to include methods for trans-lead isotopes to return to the line of stability. It is also important to compare the data from these interactions with CEMP star abundance patterns that have been shown to possess i-process material, as this will be able to tell us if our process is accurate.

2. Method

2.1 Setup

The simulation is computed with a 1-dimensional, or one-zone, code. A one-zone simulation is one that simplifies a stellar situation into a single set of parameters. This means that we can see the effect the individual parameters have on the stellar nucleosynthesis. In this case, a model using the NuGrid collaboration (Herwig et al., 2008), which is a simulation library for nuclear astrophysics, is used. The parameters that can be changed in the NuGrid model are the temperature of the star, the density of the star and the initial abundance. Temperature and density are key parameters in the reaction rates within the simulation and do not have to be constant. This type of simulation is useful as it simplifies the stellar model whilst still producing an accurate depiction, allowing for quicker simulations. However, the simulation doesn't define where in the star the reaction is taking place. The hydrodynamics within the star are also not included, which significantly affect the mixing of material. To calculate the reactions for the simulation, I used the JINA REACLIB (Cyburt et al., 2010) reaction rates, as well as reaction rates from other sources such as KADoNiS, which included all important (n,g) reaction rates up to ^{252}Cf. This includes 5627 isotopes and approximately 69000 reactions between the isotopes.

2.2 Base Run

The base run for the simulation used a temperature of 2×10^8 K, and a density of 1×10^3 g/cm^3, which are similar to that of a post-AGB star. We also have an isotopic abundance which is a standard distribution for the intershell region of an AGB star, with a large intake of hydrogen, giving the hydrogen mass fraction a value of 9×10^{-3}. This is to simulate a large intake of

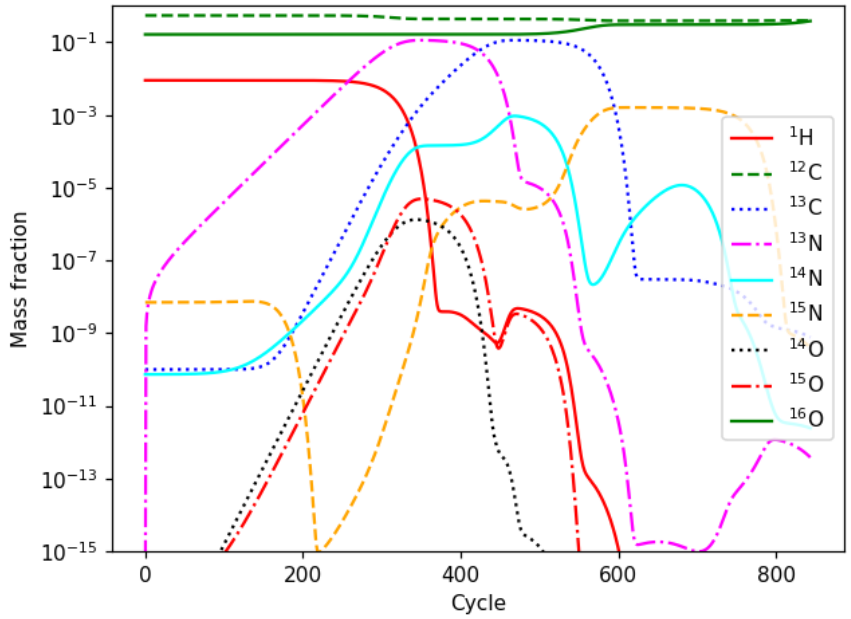

(a) The abundance of CNO isotopes with reference to cycle.

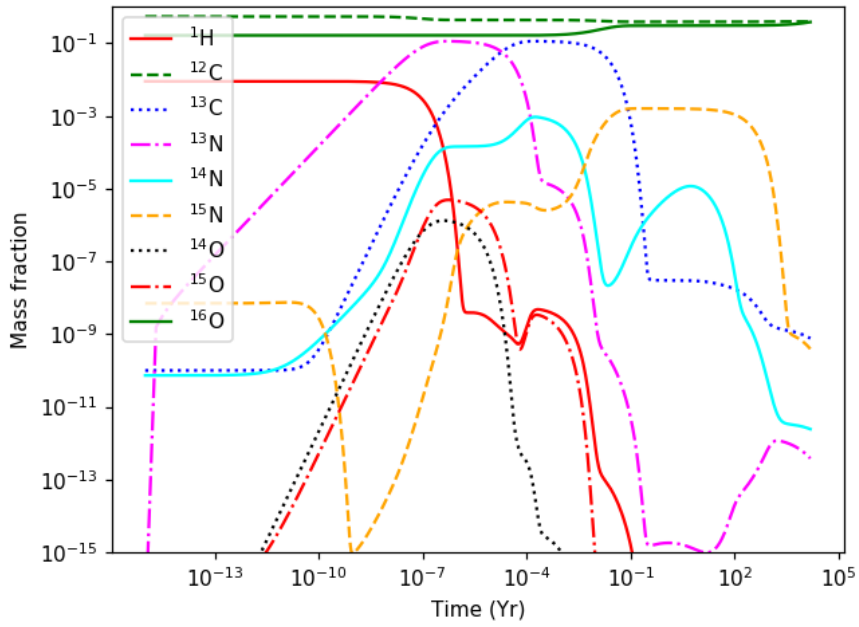

(b) Same as the figure above, but with respect to time.

Figure 2.1: This is the abundance pattern of the CNO isotopes, and from this we can see at what points certain reactions occur.

hydrogen from the hydrogen shell via convection currents within the intershell. This temperature and density is constant throughout the run to keep the simulation simple. One of the quantities effected by the temperature and density is the production of neutrons. The production of neutrons occurs when there is a series of reactions focused around carbon, nitrogen and oxygen, which is based on the CNO cycle. This can be seen in figure 2.1, which shows the abundance patterns of key isotopes around the CNO cycle, specifically how the destruction of one isotope will lead to the production of another. When ^{12}C captures a proton, it becomes ^{13}N, which then decays into ^{13}C. From here, an alpha particle is captured and a neutron is released, forming ^{16}O. This is the primary production of neutrons. When the production of neutrons is high enough, we can see the i-process in action, and when the temperature and/or density is increased, the production of neutrons is increased. However, there is a balance with the temperature. When the temperature is increased, the rate of protons captured by the ^{12}C is increased, meaning there will be more protons captured before they can decay, producing ^{14}O, which will then decay into ^{14}N. The same limitations should be seen in the change of density, except the change in density must be magnitudes more to match the change in temperature. This is because reactions scale with ρT^{ν}, so temperature is effected by other conditions. This ν value is approximately 15 for the CNO cycle.

All of the production can be seen in figure 2.1. At around cycle number 300, or 4.8×10^{-8} years, the production of ^{13}N has occurred, as we can see it rise to a mass fraction of around 5.2×10^{-2}, but we also get the production of ^{14}O, which rises to 2.6×10^{-7}, ^{14}N, which rises to 4.7×10^{-6} and ^{15}O, rising to 1.4×10^{-5}, which are all using protons and will not release neutrons afterwards. However, these values are not as significant compared to ^{13}N. At cycle 450-500, or around 3×10^{-3} years, we get the production of ^{13}C, as it rises to 1.0×10^{-1} at cycle 450, and ^{13}N decreases, as it initially falls to 1.5×10^{-5} at cycle 480, and there is a significant mass fraction for ^{13}C compared to other isotopes present. At around cycle 625, or around 3.7×10^{-1} years, ^{13}C begins to decrease down to a mass fraction of 3.1×10^{-8}, and ^{16}O increases to a value of 3.1×10^{-1} from 1.6×10^{-1}. The increase in neutrons can be seen in figure 2.2a, where we have a large increase in neutron density from 7.3×10^{-8}cm^{-3} around

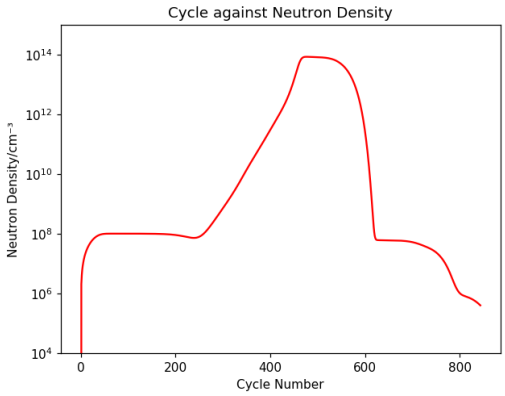

(a) Neutron density as a function of cycle number for the whole run.

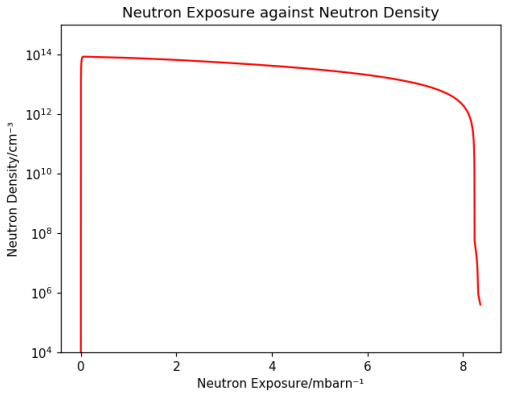

(b) Neutron density as a function of exposure.

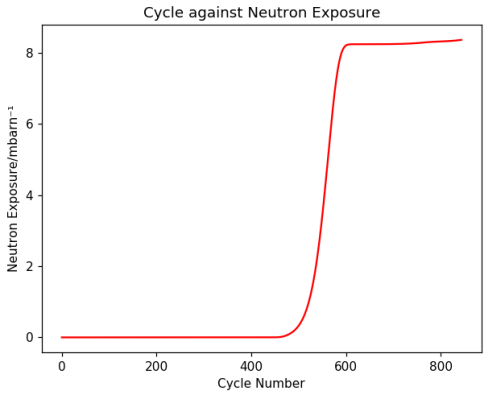

(c) The neutron exposure as a function of cycle number for the entire run. An in depth look between cycles 400 and 650 is shown in figure 2.2d, as neutron exposure change is minimal outside of this time frame.

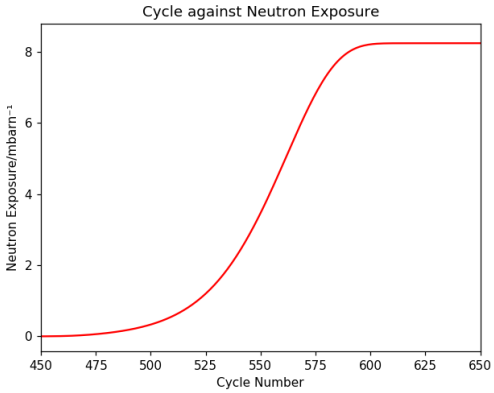

(d) The neutron exposure as a function of cycle number for between cycles 450 and 650, as this is when the neutron mass fraction is at its highest and when the most neutron captures occur.

Figure 2.2: Figures for the neutron density, neutron exposure and cycle number. Neutron density is in a logarithmic scale.

cycle number 300 (4.8×10^{-8} years) but reaching its peak value of 8.6×10^{13} around cycle 475 (2.3×10^{-4} years). Figure 2.2d shows that the neutron exposure, which refers to the neutron cross section or the probability of an interaction between a neutron and a nucleus, is still climbing at 500, we know that the neutrons have not stopped being produced at cycle 500 but are instead being used at roughly the same rate as they are being produced, and only when we get past cycle 550 is the neutron density actually decreasing.

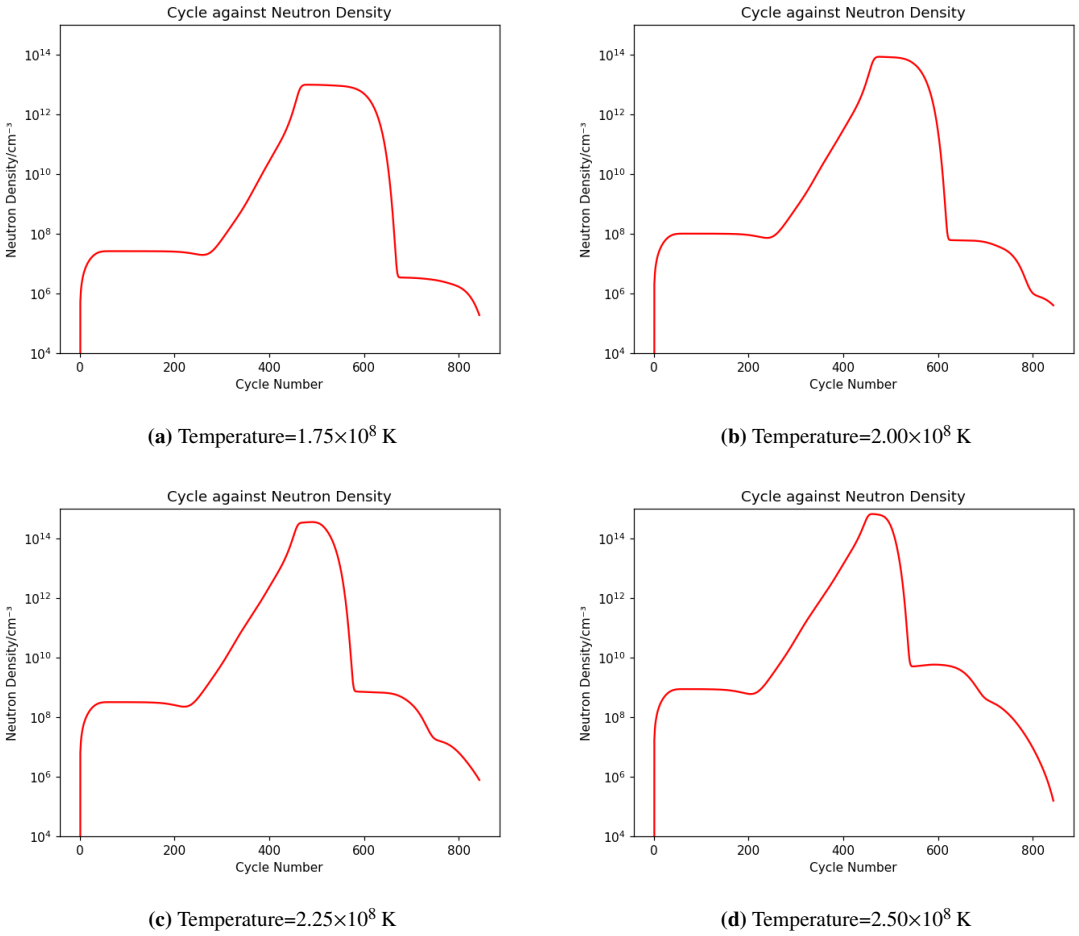

(a) Temperature=1.75×10^8 K

(b) Temperature=2.00×10^8 K

(c) Temperature=2.25×10^8 K

(d) Temperature=2.50×10^8 K

Figure 2.3: Neutron density for the different temperature runs compared to cycle number. Panel b is the base run shown before.

2.3 Temperature Changes

After running the simulation with the initial conditions, the temperature was changed to see the effect it has on the distribution of the isotopes, specifically the trans-lead isotopes. The reason for choosing temperature as the variable parameter is that it affects the reaction rates of the system. Density also affects this but not to the same degree. Starting from the initial temperature of 2×10^8 K, we varied the temperature and looked at 1.75×10^8 K, 2.25×10^8 K and 2.50×10^8 K. These temperatures have been chosen due to their proximity with the original temperature of 2.00×10^8 K, and allows for a significant range of temperatures without having to do the process more times. These values were chosen because it was important to see if the temperature would increase or decrease the mass fraction.

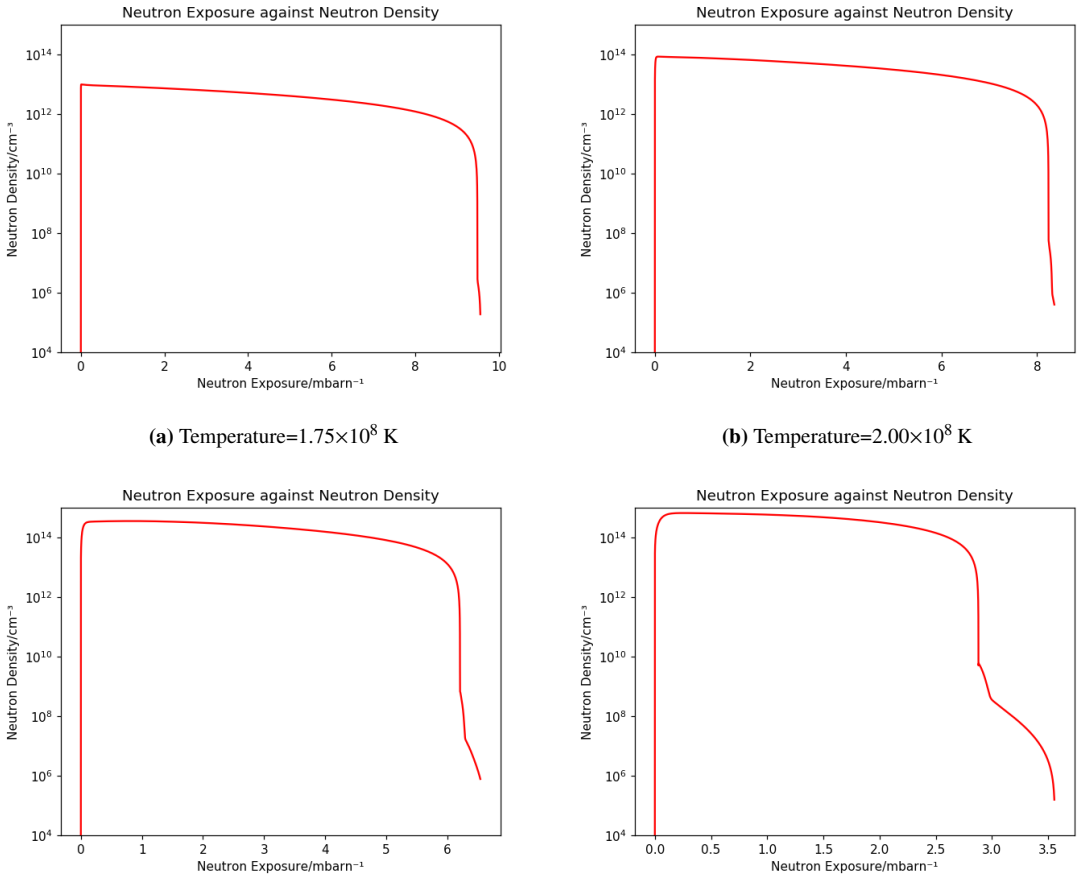

(a) Temperature=1.75×10^8 K

(b) Temperature=2.00×10^8 K

(c) Temperature=2.25×10^8 K

(d) Temperature=2.50×10^8 K

Figure 2.4: Neutron density for the different temperature runs compared with the neutron exposure. Panel b is the base run shown before.

First, we look into the neutron density of the different temperature runs, and we can see this in figures 2.3 and 2.4. These two figures show the comparisons between the neutron density over time and the neutron exposure of the runs. In figure 2.3, we see that the lower temperature run (2.3a) has a smaller neutron density throughout the entire run, being at a value of $6.7\times10^{7}\text{cm}^{-3}$ at cycle 300, compared to $7.2\times10^{8}\text{cm}^{-3}$ in the base run (2.3b). We can also see that at the peak of the run, around cycle 550, the lower temperature has a value of $9.2\times10^{12}\text{cm}^{-3}$, and the base run has a value of $4.9\times10^{13}\text{cm}^{-3}$. However, the peak neutron density for the lower temperature run stays close to $9.2\times10^{12}\text{cm}^{-3}$ for more cycles. This can be seen in figures 2.4a and 2.4b, where the density for the lower temperature is generally lower, but the exposure is larger. By the end of the run, around cycle 800, the value of the neutron density has a value of $1.7\times10^{6}\text{cm}^{-3}$ whilst the base run has a value of $1.0\times10^{6}\text{cm}^{-3}$. Generally, the neutron density of the lower temperature run is less than that of the base run. Looking at the larger temperature runs, the neutron densities for the 2.25×10^{8} K and 2.50×10^{8} K (figures 2.3c and 2.3d respectively), we see that the values are higher throughout the runs compared to the base run. At cycle 300, we have a values for the neutron density at $6.3\times10^{9}\text{cm}^{-3}$ and $4.5\times10^{10}\text{cm}^{-3}$. This is because the increased temperature also speeds the process up, so the reactions that produce neutrons occur earlier in the run. The increase in temperature also means that at the start of the run, the neutron density is a bit higher than in the base run. By cycle 550, the runs have diverged from each other due to this difference in time. Whilst the base run is still close to its peak, the other two runs are already using their neutrons to produce i-process materials, and the hottest run has just finished the majority of its i-process production. For this reason, at cycle 550, the runs with increased temperature have neutron densities of $1.0\times10^{13}\text{cm}^{-3}$ for 2.25×10^{8} K and $5.2\times10^{9}\text{cm}^{-3}$ for 2.50×10^{8} K. At cycle number 800, we see a similar trend as we did with the base run in that the neutron density reduces significantly as the run ends. The neutron densities for this cycle are, in increasing temperature, $6.4\times10^{6}\text{cm}^{-3}$ and $9.1\times10^{6}\text{cm}^{-3}$. These are slightly higher than the base run and will be because they both produce more neutrons than the base run. When we compare the neutron exposures of the hotter runs compared to the base, shown in figures 2.4c and 2.4d, we see that the the max exposure is lower than that of the base run, due to the fact that the hotter

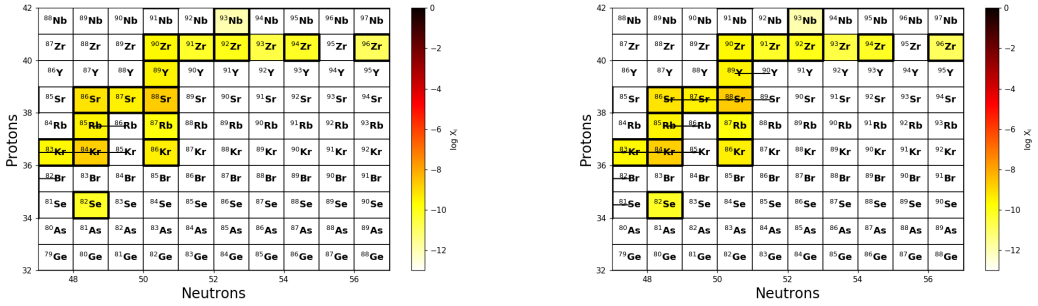

(a) Temperature=1.75×10^8 K

(b) Temperature=2.00×10^8 K

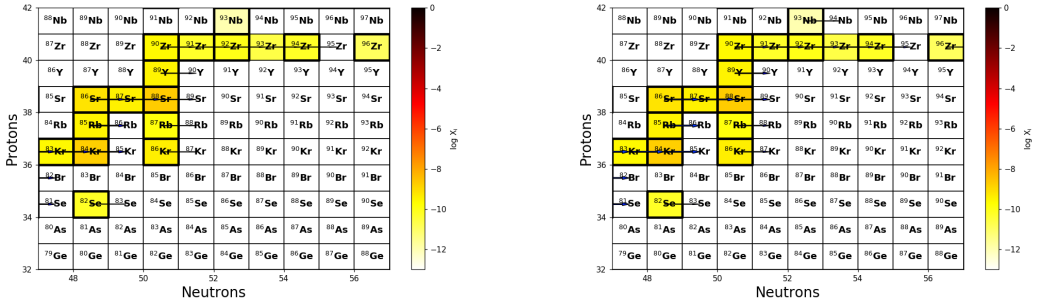

(c) Temperature=2.25×10^8 K

(d) Temperature=2.50×10^8 K

Figure 2.5: The light peak isotopes early in the runs (cycle 300) for the different temperatures, panel b is the base run shown before. Isotope mass fraction is measured by colour, with yellow being a low mass fraction and dark red being a high mass fraction. Arrows indicate the flux to and from isotopes, with thicker arrows signifying a larger flux.

temperature cause the reactions to be quicker and are not exposed to the neutrons for as long. In the case for the 2.25×10^8 K run the majority of the neutron density is before 6.2 mbarn^{-1}, whilst the 2.50×10^8 K run has its i-process exposure only up until 2.9 mbarn^{-1}, a lot less than the base runs 8.3 mbarn^{-1}.

It is important to look at the effect that the neutron production can have on the nuclide chart, especially around the neutron magic numbers. When we have a look at the light peak elements, we can see that there is not a lot of difference in the early part of the run, at around cycle 300, as seen in figure 2.5. At this time, each run has a similar neutron density and a small amount of n-capture has occurred. Therefore, when we look at the nuclide charts for these sections, there are only slight differences between the temperatures. The lower temperature (figure 2.5a) only has flux from neutron captures towards ^{85}Kr and ^{86}Rb. The higher temperatures (figures 2.5c and 2.5d) also has flux towards ^{87}Kr, ^{88}Rb, ^{89}Sr, ^{90}Y and

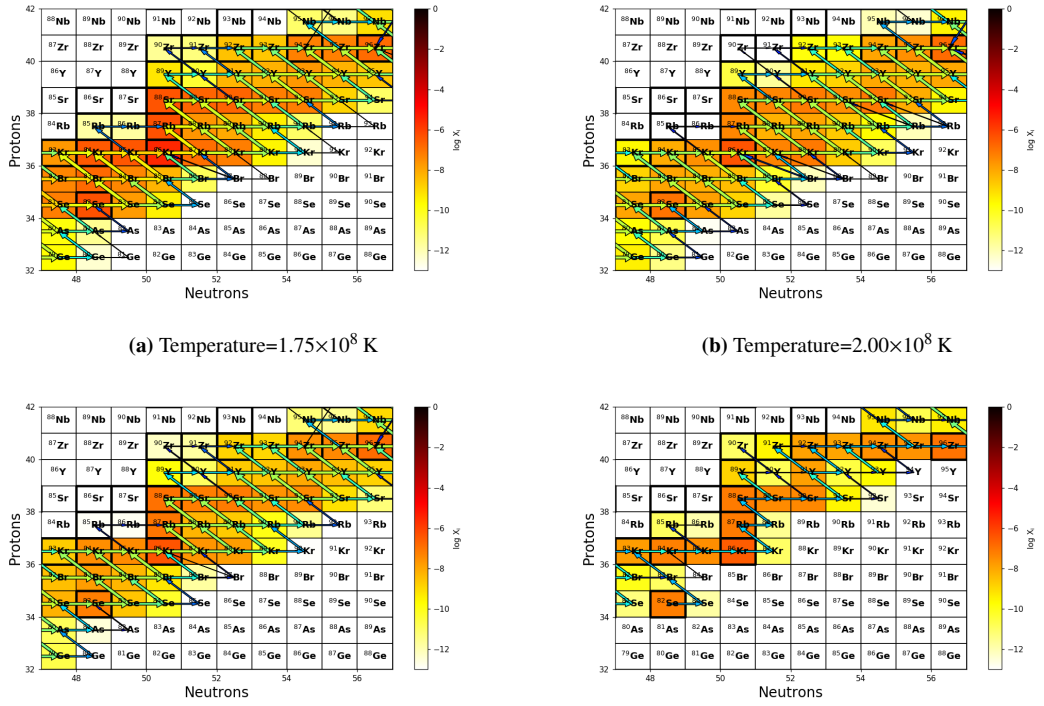

(a) Temperature=1.75×10^8 K

(b) Temperature=2.00×10^8 K

(c) Temperature=2.25×10^8 K

(d) Temperature=2.50×10^8 K

Figure 2.6: The light peak isotopes in the middle of the runs (cycle 550) for the different temperatures, panel b is the base run shown before. Isotope mass fraction is measured by colour, with yellow being a low mass fraction and dark red being a high mass fraction. Arrows indicate the flux to and from isotopes, with thicker arrows signifying a larger flux.

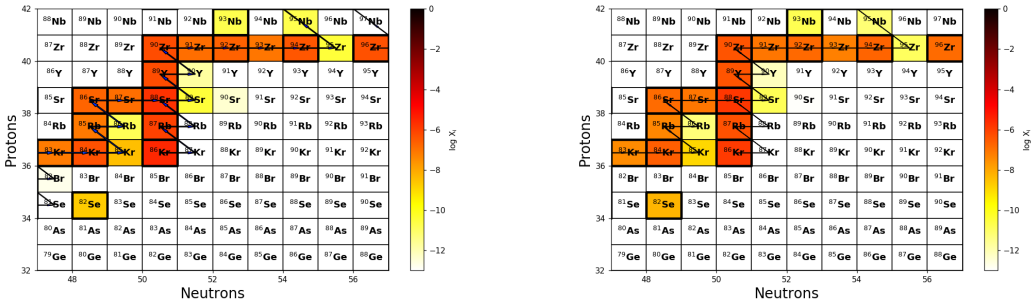

(a) Temperature=1.75×10^8 K

(b) Temperature=2.00×10^8 K

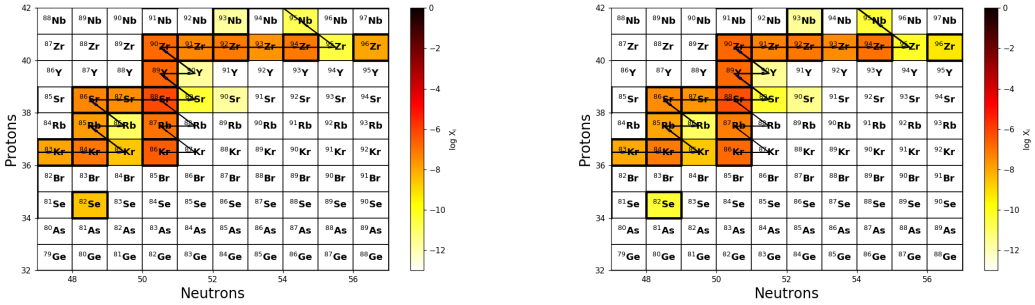

(c) Temperature=2.25×10^8 K

(d) Temperature=2.50×10^8 K

Figure 2.7: The light peak isotopes at the end of the runs (cycle 800) for the different temperatures, panel b is the base run shown before. Isotope mass fraction is measured by colour, with yellow being a low mass fraction and dark red being a high mass fraction. Arrows indicate the flux to and from isotopes, with thicker arrows signifying a larger flux.

^{91}Zr - ^{95}Zr. There is no significant change in mass fraction from the the base run (figure 2.5b). Moving on from the early section of the light peak, at cycle 550 (figure 2.6) we have a different story. At this point during the run, the neutron density has reach peak levels. Because the reaction rates rise with temperature, we can see that the cooler temperature in figure 2.6a is very similar to the base run in figure 2.6b, with only a slightly smaller production rate. We can also see that figure 2.6c is also very similar to the base run and to the cooler run, and only has slightly reduced mass fractions for the isotopes furthest from the line of stability. The hottest run (figure 2.6d) is different from the others in the fact that it has almost finished all i-process production, and is now back to something similar to the s-process production. This is because the peak neutron density occurred earlier in the simulation and has now fallen to a neutron density similar to that of the s-process. Even with this though, we can see the effects of the i-process in its production of stable isotopes which were not there in such quantity, and we should be able to see the effects better further up the nuclide chart. Finally we get to the end of the runs, at cycle 800, where the i-process has finished and the run is almost done, shown in figure 2.7. We see that all the runs look very similar to each other. There is only a slight variation in mass fractions, such as in figures 2.7a and 2.7b where the stable isotopes have a slightly larger mass fraction than in figure 2.7c and 2.7d. The fluxes are similar and isotopes with a detectable mass fraction are the same. This is because the neutron density resembles the s-process, so only small fluxes are present.

Moving on from the light peak, early on in the heavy peak (figure 2.8), the mass fraction and distribution of all the isotopes is very similar. This is because the n-density is low and nothing has happened. That has less of an effect on the heavy peak isotopes. However, what we can see is that, much like what we see at an earlier cycle in the light peak, the hotter runs (figures 2.8c and 2.8d) seem to have a little bit of a flux away from the line of stability. This is because, as previously stated, they begin their production of neutrons earlier, so have more neutrons available for neutron capture, unlike the cooler runs (figures 2.8a and 2.8b). Later on in the runs, we have at cycle 550 (seen in figure 2.9) the majority of i-process production occurring. The base run (2.9b) has a significant amount of flux moving up the nuclide chart, and significant mass fractions reaching several isotopes away from the line of stability, such

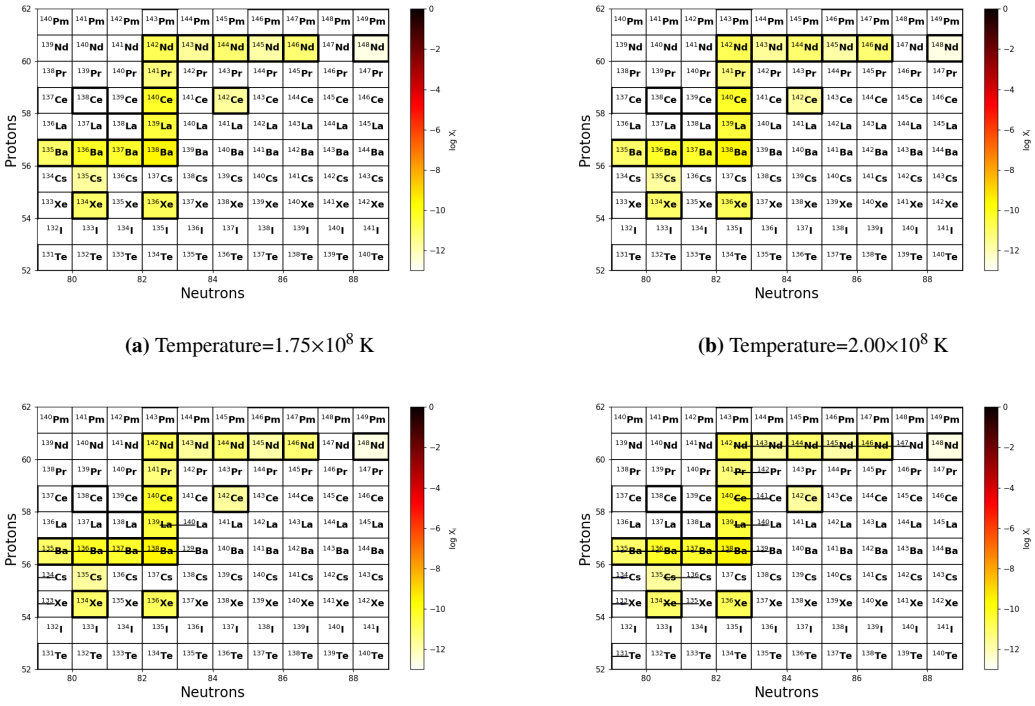

(a) Temperature=1.75×10^8 K

(b) Temperature=2.00×10^8 K

(c) Temperature=2.25×10^8 K

(d) Temperature=2.50×10^8 K

Figure 2.8: The heavy peak isotopes early in the runs (cycle 300) for the different temperatures, panel b is the base run shown before. Isotope mass fraction is measured by colour, with yellow being a low mass fraction and dark red being a high mass fraction. Arrows indicate the flux to and from isotopes, with thicker arrows signifying a larger flux.

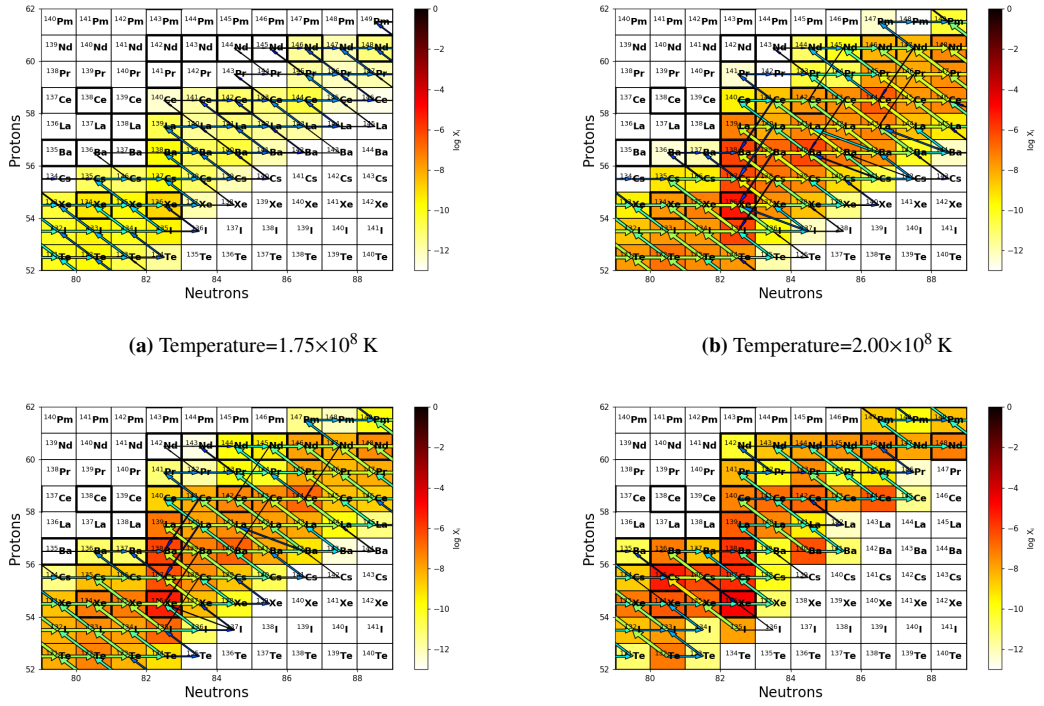

(a) Temperature=1.75×10^8 K

(b) Temperature=2.00×10^8 K

(c) Temperature=2.25×10^8 K

(d) Temperature=2.50×10^8 K

Figure 2.9: The heavy peak isotopes in the middle of the runs (cycle 550) for the different temperatures, panel b is the base run shown before. Isotope mass fraction is measured by colour, with yellow being a low mass fraction and dark red being a high mass fraction. Arrows indicate the flux to and from isotopes, with thicker arrows signifying a larger flux.

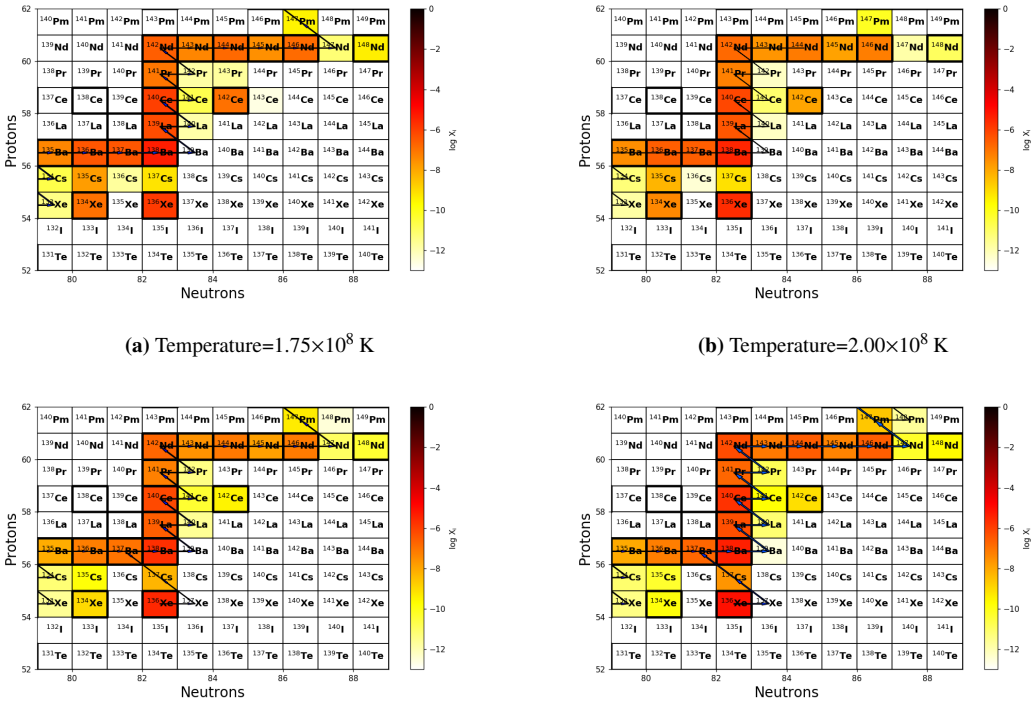

(a) Temperature=1.75×10^8 K

(b) Temperature=2.00×10^8 K

(c) Temperature=2.25×10^8 K

(d) Temperature=2.50×10^8 K

Figure 2.10: The heavy peak isotopes at the end of the runs (cycle 800) for the different temperatures, panel b is the base run shown before. Isotope mass fraction is measured by colour, with yellow being a low mass fraction and dark red being a high mass fraction. Arrows indicate the flux to and from isotopes, with thicker arrows signifying a larger flux.

as ^{138}Xe and ^{143}Ba. There are significant mass fractions in ^{136}Xe, ^{138}Ba, ^{140}Ba and ^{144}Ce, as these isotopes are more stable and have flux from (n,α) reactions depositing into them. At this cycle, we see that the production is very different due to the time disparities. We can see that in the colder run, figure 2.9a, the production has not yet reached its peak, and therefore the mass fraction for most of the isotopes, especially the i-process isotopes, is smaller than the base run (figure 2.9b). When we look at the hotter runs, we can see that in the 2.25×10^8 K run (figure 2.9c), the mass fractions and distribution is very similar to the base run, with only very minor variations. However, the difference between the base run and the 2.50×10^8 K (figure 2.9d) run is very apparent. First of all, as discussed earlier, this run is at the end of the i-process production, when the neutrons have fallen back now to s-process densities. This is why the material here is closer to the line of stability. We can also see that the isotopes have a higher mass fraction than the base due to the i-process material decaying back to the line of stability and staying there as the neutron density falls. Lastly, we see the end of the runs, figure 2.10. At this point, the i-process production has stopped and the only production is through the s-process, as seen by the flux arrows, which show that the production is only making isotopes close to the line of stability. The nuclide chart for the different temperatures are very similar, where there is not a lot of difference between the flux arrows and mass fractions for isotopes. Something of note is the difference in mass fractions for ^{142}Ce between figures 2.10a and 2.10b. The reduced neutron production in the 1.75×10^8 K run increases the mass fraction of ^{142}Ce compared to the base run. This is because the lower temperature has a lower neutron density, which means the matter concentrates around the line of stability, and does not move further up the nuclide chart. There is very little differences between the base run and figure 2.10c and 2.10d, but what we can see is a reduced mass fraction of ^{134}Xe, which arises from the reduced neutron exposure as seen in figures 2.4c and 2.4d

Finally, we get to the trans-lead section of the nuclide chart. Early in the runs, there is no production, due to the fact the original data did not have any trans-lead isotopes. This is because the simulation is the intershell of an AGB star with a hydrogen intake, and AGB stars have only undergone the s-process. Also, there is only s-process production, which does not produce trans-lead isotopes. Trans-lead isotopes are only produced when the neutron density

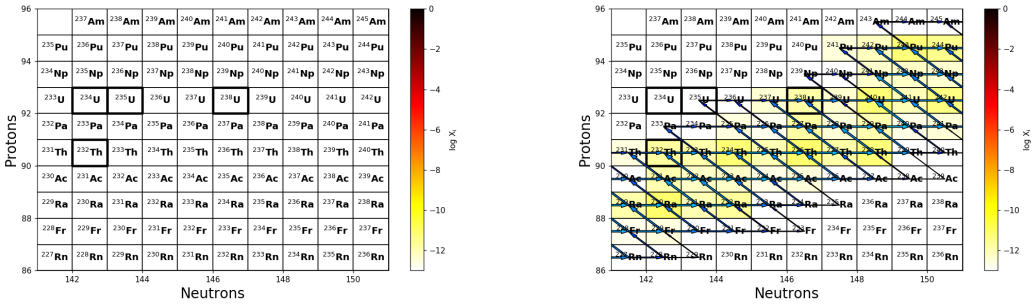

(a) Temperature=1.75×10^8 K

(b) Temperature=2.00×10^8 K

(c) Temperature=2.25×10^8 K

(d) Temperature=2.50×10^8 K

Figure 2.11: The trans-lead isotopes in the middle of the (cycle 550) runs for the different temperatures, panel b is the base run shown before. Isotope mass fraction is measured by colour, with yellow being a low mass fraction and dark red being a high mass fraction. Arrows indicate the flux to and from isotopes, with thicker arrows signifying a larger flux.

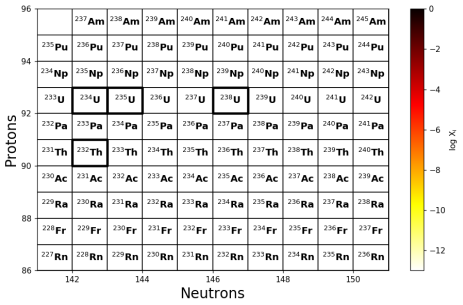

(a) Temperature=1.75×10^8 K

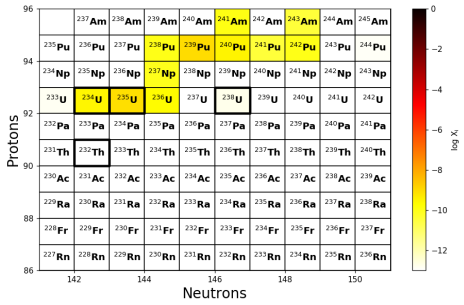

(b) Temperature=2.00×10^8 K

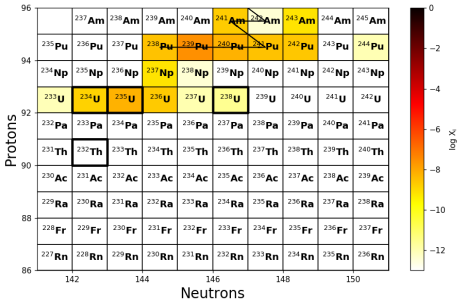

(c) Temperature=2.25×10^8 K

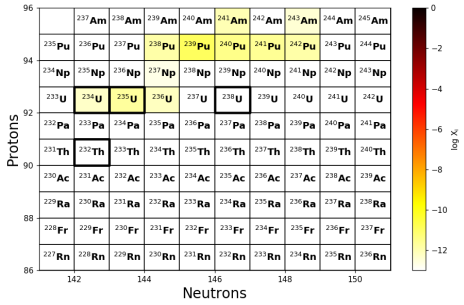

(d) Temperature=2.50×10^8 K

Figure 2.12: The trans-lead isotopes at the end of the runs (cycle 800) for the different temperatures, panel b is the base run shown before. Isotope mass fraction is measured by colour, with yellow being a low mass fraction and dark red being a high mass fraction. Arrows indicate the flux to and from isotopes, with thicker arrows signifying a larger flux.

is high enough. Here they are not made until close to the neutron density peak. Moving on from the early section of the run, the middle of the run, at cycle 550 (figure 2.11), shows the i-process production in progress. The production of trans-lead isotopes does not occur in both the coldest and the hottest runs (figures 2.11a and 2.11d). In the colder run, this will be because the reactions are too slow so they never reach up to the trans-lead isotopes, meanwhile in the hotter run, the production has already occurred and passed this section of the nuclide chart, which we know because we can see it later on. When we look at the other hot run, figure 2.11c, we can see that there is some production of trans-lead isotopes but they are much less than the base run (figure 2.11b). This is caused by the temperature increasing the reaction rates, and that the hotter run is further in its i-process production phase. When we look at the end of the run, shown in figure 2.12, we can see once again that the colder temperature run, figure 2.12a, there is no production of trans-lead isotopes. What we do see is a presence of these trans-lead isotopes in both of the hotter temperature runs. Looking at figure 2.12d, we can see the production of the trans-lead isotopes. As they decay back towards lead and the line of stability, as they head back down, they collect at the quasi-stable uranium isotopes, particularly ^{234}U and ^{235}U, with values of around 1×10^{-8} for the $2.25{\times}10^{8}$ K run and around 1×10^{-11} for the $2.50{\times}10^{8}$ K. However, the production of these trans-lead isotopes is not to the same degree that the base run seems to have been, and therefore the mass fraction of these isotopes is not as much as what can be seen in figure 2.12b. In figure 2.12c, we can see that the production of these trans-lead isotopes is more significant that in the base run, and therefore we have larger mass fractions for all the isotopes that are present in the base run. Some of the isotopes are shown in this run that do not show up in the base run, such as ^{238}U, or the mass fraction in the base run is too small to show on the nuclide chart. This run is also the only run to show any flux arrows, however small, in the late stage of the data. The lack of flux arrows show that the decays are happening over a very long period of time.

An important side note is that the run at $1.75{\times}10^{8}$ K does not produce any isotopes at the top end of the nuclide chart. We can see this in figure 2.13a, which shows the nuclide chart around ^{208}Pb at 10^{-2} years. The dark squares show a larger mass fraction for the isotopes, and the size of the flux arrows show the amount transferring into and out of the isotopes. What

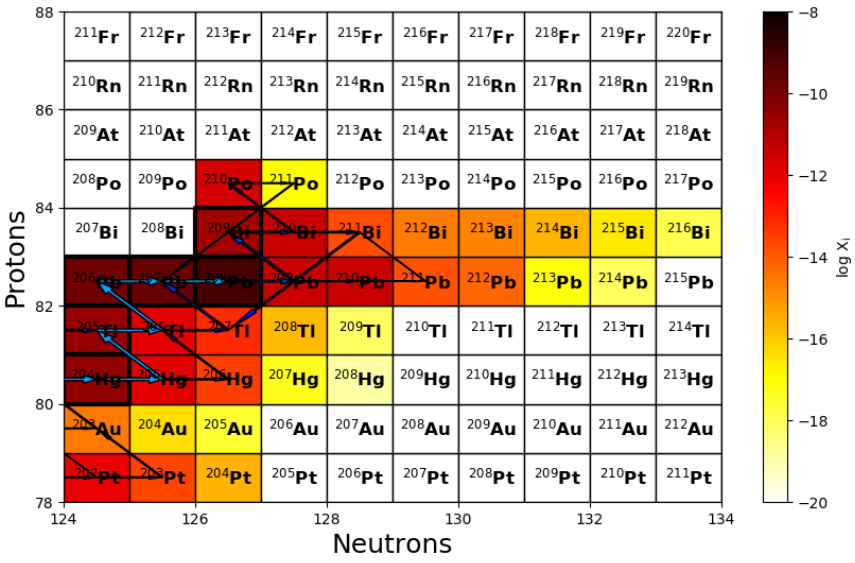

(a) Temperature=1.75×10^8 K

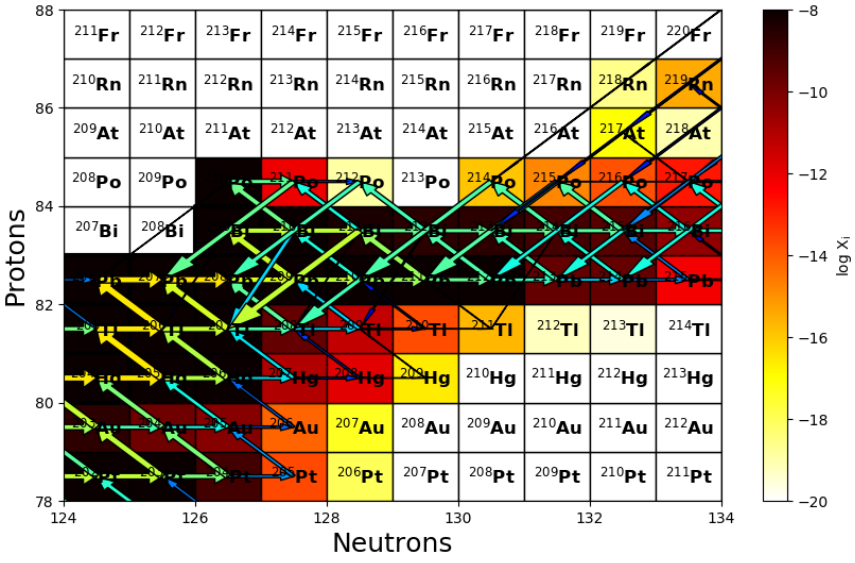

(b) Temperature=2.00×10^8 K

Figure 2.13: The section of the nuclide chart located around lead, specifically ^{208}Pb and occurred at 10^{-2} years (cycle 550). The limit on the chart has been changed to show the production for this section. Isotope mass fraction is measured by colour, with yellow being a low mass fraction and dark red being a high mass fraction. Arrows indicate the flux to and from isotopes, with thicker arrows signifying a larger flux.

we see is the production of unstable lead, bismuth and polonium. However, the production stops before we can produce anything heavier. This is due to the reduced neutron density caused by the lower temperature. The neutron density for this temperature only reaches $1.00 \times 10^{-13} \mathrm{cm}^{-3}$ which is lower than the other runs. All other runs reach higher than this and produce isotopes higher up the nuclide chart. The reason why this run does not reach further up the nuclide chart would be due to the half-lives of the bismuth and polonium isotopes, as well as the way these isotopes decay. ^{212}Bi to ^{218}Bi, undergo β- decay and have half-lives in the range of minutes and seconds, meaning they will decay towards polonium. The polonium isotopes involved have short half-lives, in the range between minutes and micro-seconds, and undergo α decay. Compare that to the same section of the nuclide chart at the same time but for the base run (figure 2.13b), and we can see that, although we have an increase in the amount that follow the same decay path, we also see a large mass fraction capture additional neutrons, which will then allow those atoms to climb the nuclide chart. This is due to the increase in neutrons between the two runs.

3. Introducing neutron-induced fission reactions

The upper section of the nuclide chart, beyond lead, has no stable isotopes and only a few quasi-stable isotopes, such as isotopes whose half-lives are longer than 10^6 yrs, mentioned previously. All of these isotopes are unstable and will decay back to stability, given enough time. Along with (n,g) and α decay reactions present in the original network, one of the main ways the trans-lead isotopes undergo destruction is by neutron induced fission, hereafter (n,f), the act of a nucleus capturing a neutron and causing a fission reaction to break up the heavy nuclei. This destruction can form two or more daughter nuclei, as well as a number of neutrons, which will have to be discussed further. This fission reaction does not produce definitive daughter nuclei, and follows a probability distribution in the nuclei they produce. To implement the neutron fission reactions into the simulation, the daughter nuclei were simplified so that a single unstable isotope would only ever produce two daughter nuclei. This is for computational convenience as the code is more capable at performing two-body reactions. The new daughter nuclei would take the mass of the unstable nucleus and divide the protons and neutrons of a nucleus in a 3:2 ratio. An example of this would be ^{235}U, which splits into ^{142}Ba and ^{94}Sr. This ratio was used as it seemed to distribute the daughter nuclei across the lower section of the nuclide chart, not affecting the production in these sections. We can see roughly similar distributions in Panov et al. (2010), so this assumption is reasonable. This increase in pre-lead isotopes is very small and will only occur after the production of post-lead isotopes which is during and after the peak neutron density, so will not affect the upper section as opposed to α decay, which still decays into post-lead isotopes. This simplification does not produce any additional neutrons from the decay. Therefore, the daughter nuclei produced are more neutron heavy and will decay quickly back to the line of stability where they will then capture more neutrons. Another simplification was in the amount of isotopes that included the neutron fission reaction rates. The production of isotopes was done via neutron capture, and so isotopes that were proton heavy did not need to have

their (n,f) rates included. The isotopes that are produced only capture a certain number of neutrons before decay is certain due to a short half-life, so any isotopes that fall outside of this limit also do not have their (n,f) rates included. Reaction rates for the neutron fission were taken from Table 18 of Panov et al. (2010)

3.1 Importance of neutron induced fission reactions

The introduction of the (n,f) rates is necessary for the upper section of the nuclide chart. In this section, isotopes decay in several ways: α decay, β- decay and neutron-induced fission. α decay is when the isotope is too large and has to decay back to a more stable isotope. This occurs in some of the trans-lead isotopes such as ^{236}U and ^{246}Cm. β- decay, which we have discussed, is caused by the i-process in this section of the nuclide chart and not the s-process. Neutron-induced fission, the reaction in which a nucleus captures a neutron and then splits into smaller isotopes, is imperative in modelling the upper section of the nuclide chart. The base run produces lots of material in the upper section of the nuclide chart, but the introduction of fission reactions, an important part of the physics of this section, is lacking. By including these rates, we can model the upper section of the nuclide chart more accurately, and we expect the nuclei will not accumulate at the top of the nuclide chart due to the inclusion of the (n,f) rates. Nucleosynthesis is a competition between the (n,g) rates producing heavier isotopes, and the (n,f) rates destroying them. We can look at the relative importance of the two by comparing the rates. Not all (n,f) rates will be important, for some, the (n,f) make up only a small percentage of their total destruction, such as ^{251}Bk, and some do not fall in the i-process production path, such as ^{232}U. In table 3.1, we see the significant relevance each destruction path has on the total destruction of that isotope at a temperature of 2×10^8 K, by using the ratio of the (n,g) to (n,f) rates from (Panov et al., 2010). From what we see in the table, certain isotopes may make a significant difference to the outcome of the isotopic abundances at the top of the nuclide chart, as their respective (n,g) to (n,f) ratio is large enough that the introduction of the isotope will change the output abundance. For example, ^{241}Pu has a JINA Reaclib (n,g) rate of 6.653e+06 s^{-1} and an (n,f) rate of 7.097e+08 s^{-1}, giving a ratio of 1.067e+02. Significant isotopes are ^{241}Pu, ^{243}Pu, ^{245}Cm and ^{251}Cf, and the relevant

ratios can be seen in figure 3.1. Figure 3.1 shows the relation between temperature and the reaction rates, two (n,g) rates, one from table 10 of (Panov et al., 2010) and the other from JINA Reaclib (Cyburt et al., 2010), and the (n,f) rates from (Panov et al., 2010). The inclusion of two (n,g) rates is to compare them to each other, ensuring the accuracy of the tables in Panov et al. (2010) . The figures show the (n,f) rates at least one magnitude higher than the (n,g) rates. It should be noted that although ^{241}Pu has a high ratio, it is less important as it is not on the i-process path. We also only care about those isotopes above uranium as only after do we see a significant (n,f) rate. However, some isotopes are also insignificant when it comes to their (n,g) to (n,f) ratio, and as such the (n,f) rates are unlikely to affect the outcome of the isotopic abundances at the top of the nuclide chart. Examples of these isotopes are ^{248}Pu, ^{247}Am, ^{251}Bk and ^{252}Bk, shown in figure 3.2, which uses the same relevant data as figure 3.1. These graphs show that, at the temperature we are looking at, which is around $T = 10^{-1}\,T_9$ where $T_9 = 10^9$ K, the (n,f) rates are several orders of magnitude below that of both the (n,g) from (Panov et al., 2010) and the JINA Reaclib rates. It is important to note that for the temperature range we are looking at, the difference between the two (n,g) rates does not matter, as any isotope with a significant (n,f) rate has similar (n,g) rates. We therefore expect isotopes such as ^{241}Pu, ^{243}Pu, ^{245}Cm and especially ^{251}Cf to be important. ^{251}Cf and ^{252}Cf are at the end of the nuclide chart and with ^{251}Cf having such a high ratio of (n,f) to (n,g) rates. From the analysis of the runs without the (n,f) rates, we found a large build up in these isotopes and the introduction of the (n,f) rates should deplete the pile-up of abundance.

3.2 Effects of (n,f) reactions

By adding the (n,f) rates shown in tables A.4 and A.5, we can re-run the simulations to determine how they affect the nucleosynthesis. We start by describing the changes in the base run. The difference between the base run and the run after the introduction of the (n,f) rates shows that the (n,f) rates do change the outcome of the isotopic abundances. Figure 3.3 shows the production of key isotopes around the ls peak, hs peak, quasi-stable trans-lead isotopes and the end of the nuclide chart. Each figure shows the production of the base run (indicated by the dashed lines) and the (n,f) run (indicated by the solid lines). In all of the panels seen

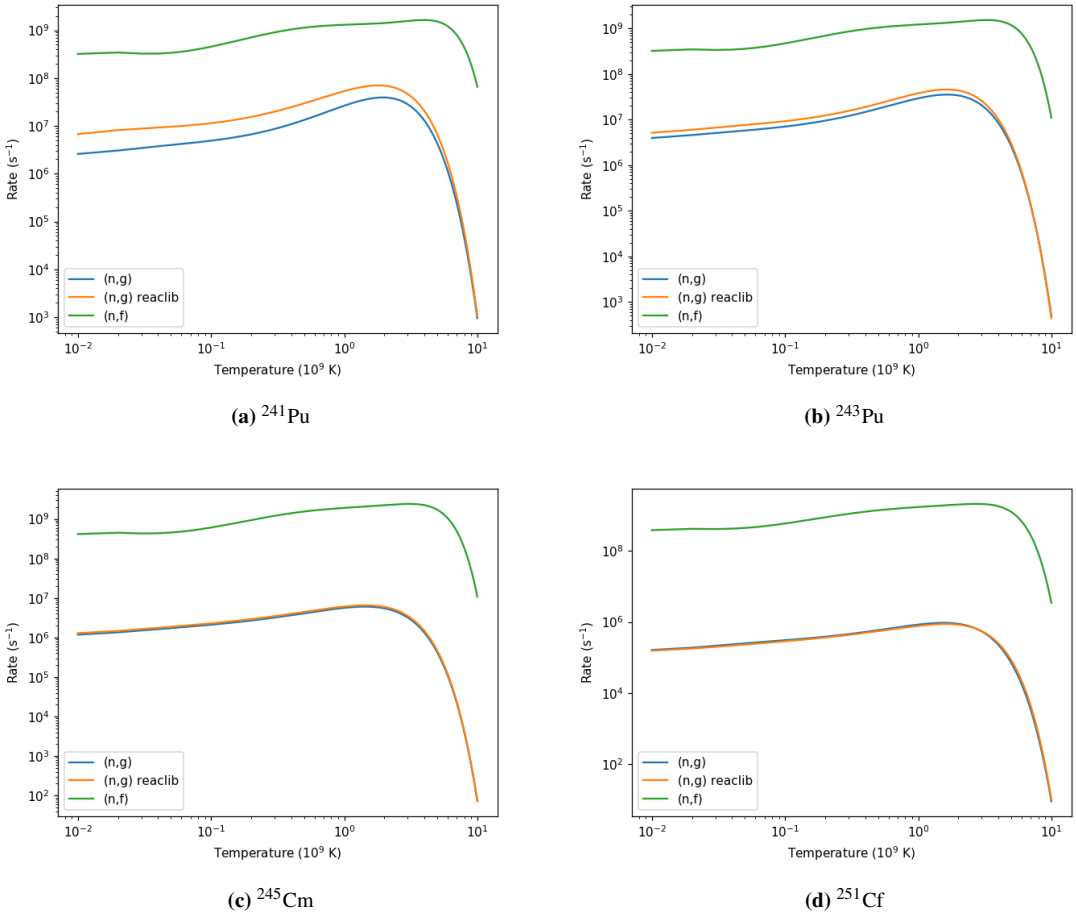

(a) ^{241}Pu **(b)** ^{243}Pu

(c) ^{245}Cm **(d)** ^{251}Cf

Figure 3.1: Examples of isotopes that show the significance of the introduction of the (n,f) rates. The graphs show the reaction rate with regards to temperature. The blue and orange lines represent the (n,g) rates from (Panov et al., 2010) and JINA REACLIB respectively. The green is the (n,f) rates from (Panov et al., 2010).

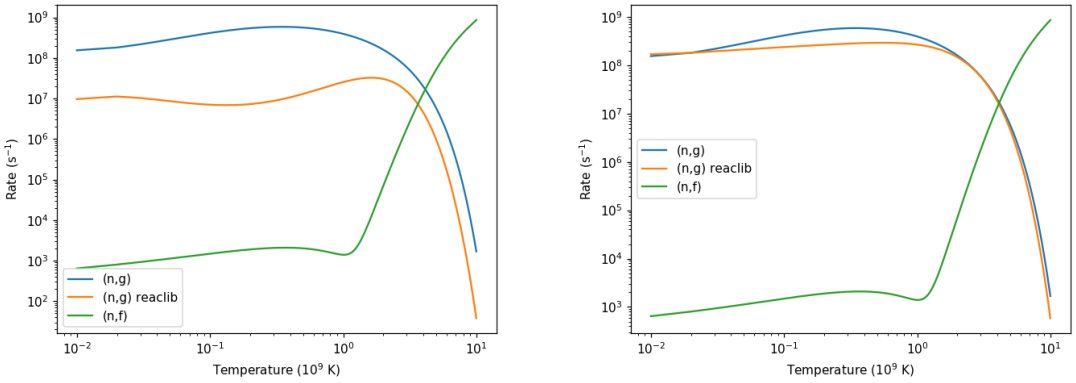

(a) ^{248}Pu **(b)** ^{247}Am

(c) ^{251}Bk **(d)** ^{252}Bk

Figure 3.2: Examples of isotopes that show some insignificance of the introduction of the (n,f) rates. The graphs show the reaction rate with regards to temperature. The blue and orange lines represent the (n,g) rates from (Panov et al., 2010) and JINA REACLIB respectively. The green is the (n,f) rates from (Panov et al., 2010).

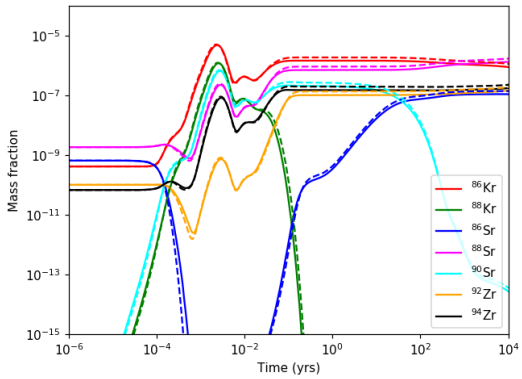

(a) Comparison of key isotopes around the light peak isotopes.

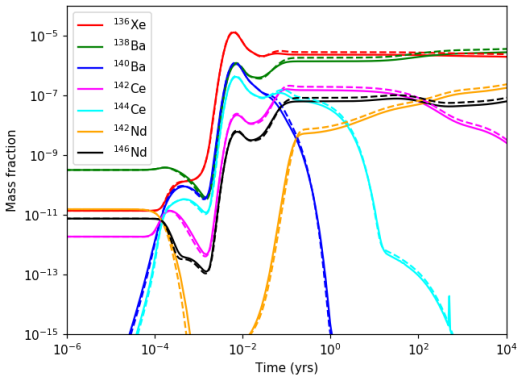

(b) Comparison of key isotopes around the heavy peak isotopes.

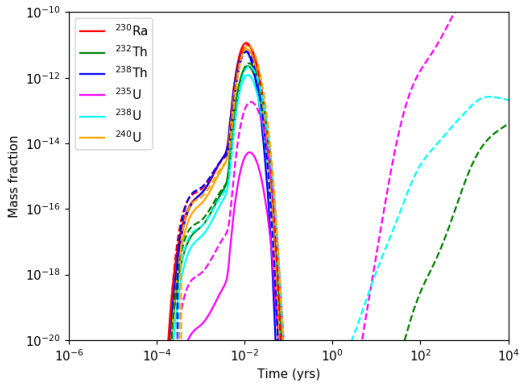

(c) Comparison of key isotopes around the quasi-stable trans-lead isotopes.

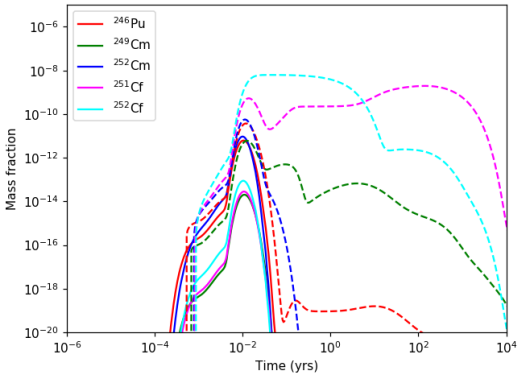

(d) Comparison of key isotopes at the top of the nuclide chart.

Figure 3.3: Comparisons between the base run before the introduction of the (n,f) rates, shown with the dashed lines, and after the introduction of the (n,f) rates, shown with the full lines. Both runs have the same initial conditions.

in figure 3.3, the starting time is at 10^{-6} years as there is no differences before this time on any of the graphs. We see a minor change in the mass fractions of the isotopes in both the light and heavy peak isotopes. Focusing on the light peak, particularly isotopes that have a large build up in the base run (^{86}Kr and ^{90}Sr), as well isotopes that are on or around the magic neutron number (^{88}Sr and ^{90}Zn), shown in figure 3.3a, we can see that close to the start of the run, the difference between the base run and the (n,f) run is insignificant. It is only until we get to around 10^{-4} years, where the isotopes start to react that we see any differences in the two runs. Even though there are some differences, we only see it when the isotopes drop below a mass fraction of 10^{-10}, which indicates that the difference is not substantial and the mass fraction difference between the two runs is at most 1×10^{-12}. Later on near the end of the run, at around 2×10^{-2} years, the light peaks have changed very little from each other, but this is the point when they do diverge. The largest difference is a mass fraction of 4×10^{-7}, seen in ^{86}Kr, with the base run being slightly higher than the (n,f) run. There is approximately 1 magnitude difference between the base run and the (n,f) run for ^{86}Kr, which is a trend seen in all the other isotopes from figure 3.3a. Isotopes from the (n,f) run follow the same pattern as their respective isotope in the base run.

The isotopes around the heavy peak, much like the light peak, show little difference between the two runs, which can be seen in figure 3.3b. The isotopes chosen were those with high mass fractions (^{144}Ce and ^{146}Nd), or those which lie on the neutron magic number (^{136}Xe and ^{138}Ba). Early on in the runs, we only see a difference between the runs when the mass fraction goes below a certain level, and even when we see this change, the values are at most a mass fraction of 2×10^{-13}. This continues until 3×10^{-2} years, when once again the runs diverge from each other and the base run is slightly higher than the (n,f) run, this time by at most 5×10^{-7}. Once again, throughout the runs, matching isotopes have the same pattern as each other. As we can see from both the light and heavy peaks, the introduction of (n,f) isotopes has little effect on the overall production of isotopes lower down in the nuclide chart. This is because the introduction of the (n,f) rates is only in the upper section of the nuclide chart, and the only real effect will be the daughter nuclei produced by the (n,f) decays, which will most likely get carried back up the nuclide chart as they reach the i-process material.

This is also because the trans-lead isotopic abundances are low, so even with the destruction, there will not be a large quantity being returned to the lower part of the nuclide chart.

The trans-lead isotopes are effected by the introduction of (n,f) rates, as shown in figures 3.3c and 3.3d. Looking at the quasi-stable isotopes (figure 3.3c), we see that the production of these isotopes occurs around 10^{-4} years into the run. Here we can see the first differences between the runs. All isotopes selected here, especially ^{235}U, have a difference between runs. The largest difference between runs in terms of ratio would be from ^{235}U, which at its peak mass fraction at 1.2×10^{-4} years, has a difference of almost 2 orders of magnitude, from a mass fraction of 1.9×10^{-13} in the base run, to mass fraction of 5.2×10^{-15} in the (n,f) run. This is shown in table 3.1, where we can see that the (n,g) to (n,f) ratio for ^{235}U is 34.68. If we also take into account some of the material that would have made it to ^{235}U has already undergone neutron-induced fission, then we should expect to see this difference. Another important factor in figure 3.3c is the section after 1 year. Here we can see that production for ^{232}Th, ^{235}U and ^{238}U increases in the base run and not in the (n,f) run. This is caused by the material decaying from the upper limit of the nuclide chart (figure 3.3d) down to these isotopes. This is a notable distinction from the (n,f) run, where the neutron-induced fission causes that material to be recycled back into the lower sections of the nuclide chart. Therefore, the ^{232}Th, ^{235}U and ^{238}U in the (n,f) run will not have these production peaks.

It is also important to look at the very top of the nuclide chart, as the production and fission of these isotopes is important to the overall abundance of the quasi-stable trans-lead isotopes. This is because as the very large trans-lead isotopes undergo α decay, they travel to the quasi-stable isotopes where they will accumulate. This section can be seen in figure 3.3d. Much like before, the production starts at around 10^{-4} years, and they all have a difference between runs. At the peak production (10^{-2} years), ^{246}Pu and ^{252}Cm have the smaller mass fraction differences of 2.4×10^{-11} and 4.1×10^{-11} respectively. These two isotopes show the reduced production of the upper section of the nuclide chart due to the neutron-induced fission of isotopes lower down the nuclide chart and a small ratio of (n,g) to (n,f) rates seen in tables 3.1 and 3.1. However, ^{249}Cm, ^{251}Cf and ^{252}Cf have very large differences in mass fraction, with differences of 2, 4 and 5 orders of magnitude respectively. This will again be

Isotope	(n,g) rate (s^{-1})	(n,f) rate (s^{-1})	ratio
^{232}Th	3.279e+07	4.151e+02	1.266e-05
^{235}U	1.346e+07	4.669e+08	3.468e+01
^{238}U	3.410e+07	1.626e+03	4.767e-05
^{241}Pu	6.653e+06	7.097e+08	1.067e+02
^{246}Pu	5.025e+07	4.095e+06	8.149e-02
^{249}Cm	9.945e+06	6.222e+08	6.257e+01
^{252}Cm	7.623e+07	4.551e+04	5.971e-04
^{251}Cf	3.851e+05	8.887e+08	2.308e+03
^{252}Cf	6.464e+06	2.293e+08	3.548e+01

Table 3.1: Important reaction rates at a temperature of T=2 $\times$ 10^8 K for (n,g) and (n,f) for trans-Pb isotopes as taken from tables 10 and 18 of Panov (respectively), together with their ratio, (n,f)/(n,g).

caused by the reduced production of the isotopes from earlier neutron-induced fission, but also because these isotopes have a higher ratio of (n,g) to (n,f) rates seen in figure 3.1. As the isotopes move past the peak abundances, we can see that the (n,f) run drops off very quickly as production is stopped and the neutron-induced fission reduces the mass fraction. This is not present in the base run, where the α decay of these isotopes take a long time and will fall down to the quasi-stable isotopes.

3.3 Effects of the (n,f) reactions with changing temperature

To investigate the temperature dependence of the (n,f) rates, the (n,f) rates simulation has been run at 2.25$\times$$10^8$ K and 2.50$\times$$10^8$ K. Both of these temperatures have little difference in their light and heavy peaks, and look similar to that of the 2.00$\times$$10^8$ K light and heavy peaks. We focus on discussing the trans-lead isotopes. Starting with the 2.25$\times$$10^8$ K run, figure 3.4 shows the comparison for the trans-lead isotopes between the base (n,f) run and the 2.25$\times$$10^8$ K (n,f) run, with figure 3.4a being around the quasi-stable isotopes, and figure 3.4b for the end of the nuclide chart. What we see from these figures is that the production of material at the

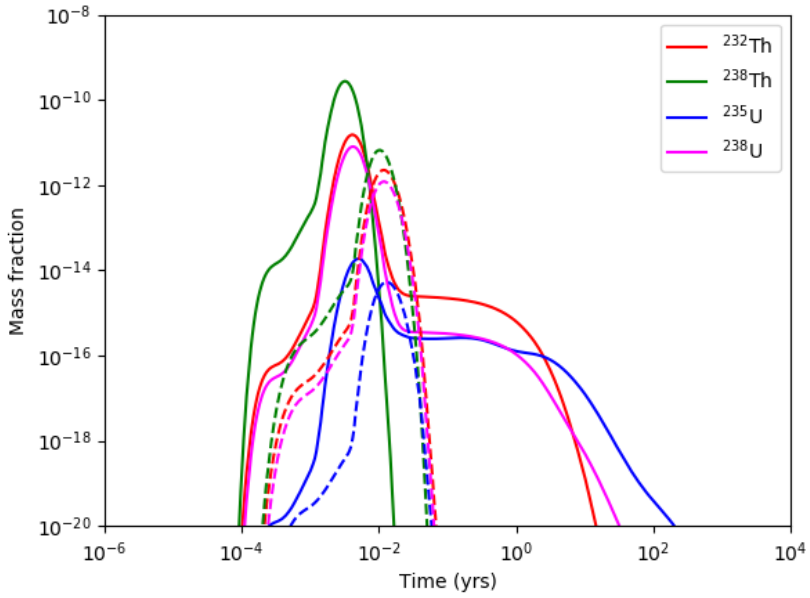

(a) Comparison of key isotopes around the quasi-stable trans-lead isotopes.

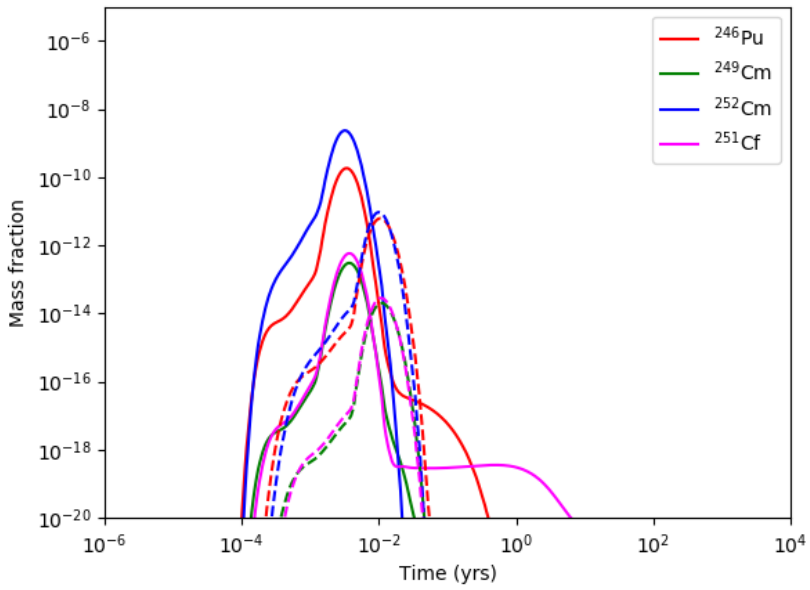

(b) Comparison of key isotopes around the upper end of the nuclide chart.

Figure 3.4: Comparison between the 2.25×10^8 K (n,f) run and the 2.00×10^8 K (n,f) run. The dashed lines represent the 2.00×10^8 K (n,f) run, and the full lines represent the 2.25×10^8 K (n,f) run.

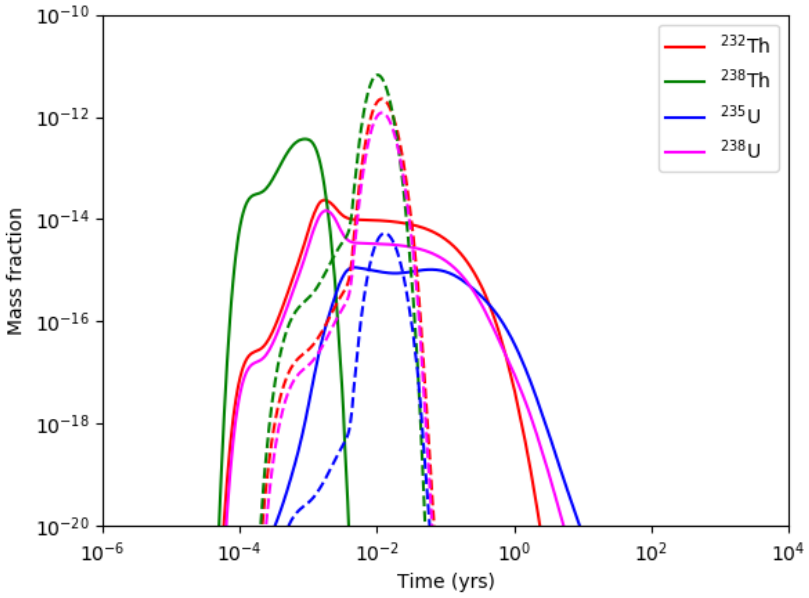

(a) Comparison of key isotopes around the quasi-stable trans-lead isotopes.

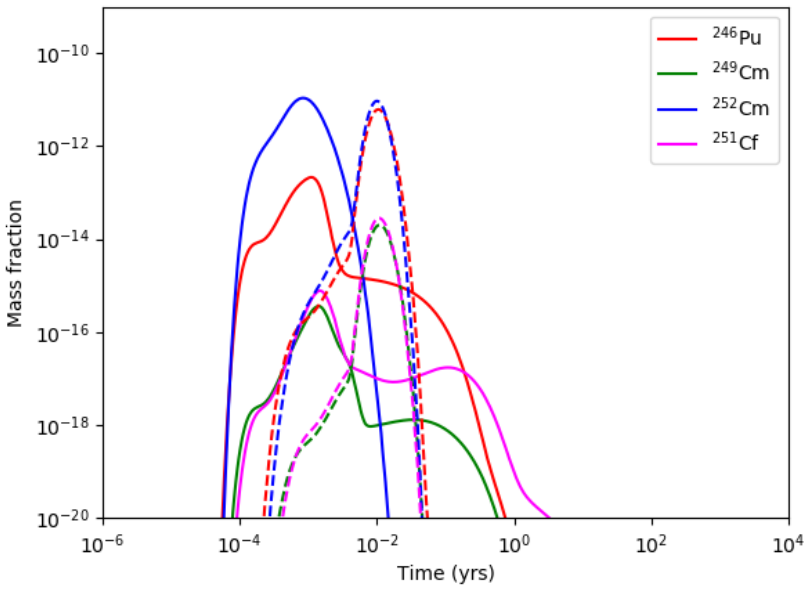

(b) Comparison of key isotopes around the upper end of the nuclide chart.

Figure 3.5: Comparison between the 2.50×10^8 K (n,f) run and the 2.00×10^8 K (n,f) run. The dashed lines represent the 2.00×10^8 K (n,f) run, and the full lines represent the 2.50×10^8 K (n,f) run.

higher temperature has been shifted to earlier times. This is due to the production of neutrons occurring earlier and being more intense. The shift in the peak abundance for the isotopes is from 1×10^{-2} to 3×10^{-3} years. The increase in the peak mass fraction for the $2.25{\times}10^{8}$ K run is over two orders of magnitude larger than the base run. Another feature of the $2.25{\times}10^{8}$ K run is a balance in the production and decay of the isotopes soon after the peak mass fraction. This feature occurs for several of the isotopes shown, and does not appear for any isotopes in the base run. This does occur in the base run but at several magnitudes lower. When we compare this to the non-(n,f) runs of the same temperature, the (n,f) runs have lower mass fractions across all isotopes shown. The comparison between the $2.50{\times}10^{8}$ K (n,f) run and the base run can be seen in figure 3.5, with the comparison of isotopes around the quasi-stable isotopes shown in figure 3.5a and the comparison of isotopes at the upper end of the nuclide chart. Much like in the comparison for the $2.25{\times}10^{8}$ K (n,f) run, in both of these figures, the reaction rates for the $2.50{\times}10^{8}$ K (n,f) run occurs earlier, with a peak mass fraction occurring one magnitude earlier than in the base (n,f) run. This is to be expected as the increased temperature increases the reaction rate of the system. We also see that the production of ^{252}Cm matches that of the base run, but other isotopes have a lower peak mass fraction due to the reduced production of neutrons in the higher temperature run. We once again see the production in the higher temperature balancing out with the destruction after the peak mass fraction, with the balance occurring at 10^{-2} years. Comparing this to the $2.25{\times}10^{8}$ K (n,f) run, the levelling out occurs earlier due to the increased reaction rate. However, the levelling out occurs at a higher value, as we can see from ^{232}Th, where the hotter run levels out just above 10^{-14} mass fraction, and the cooler run levels out just below 10^{-14} mass fraction. This pattern of the $2.25{\times}10^{8}$ K (n,f) run levelling lower than the $2.50{\times}10^{8}$ K (n,f) run is also seen in ^{238}U, ^{246}Pu, ^{249}Cm and ^{251}Cf.

4. Discussion

4.1 HE 0338-3945

It is important to look at real-world examples of the effects of i-process sites and determine whether the production of trans-lead isotopes could be explained using the i-process. In order to do this, the star HE 0338-3945 (Jonsell et al., 2006) was chosen as a good candidate, due to the presence of trans-lead isotopes in the stars spectral analysis and a combined s and r process abundance pattern, which can be linked to the i-process, as seen in Hampel et al. (2016). HE 0338-3945 has an [X/Fe] upper limit value for thorium of <2.57 and an [X/Fe] upper limit value for uranium of <2.82. The upper limits for these two elements are because of the uncertainty present in the spectral analysis, due to the presence of other elements with similar spectral lines blending with the ones we want. The thorium upper limit was based on a single spectral line, with a fairly reliable upper limit. However, uranium did not have a detectable spectral line, so the upper limit was derived by other factors and depends on the modelling used. The presence of trans-lead isotopes is uncommon to see, and with significant values, it is possible to compare the star to the data which has been produced earlier on in this thesis.

To determine whether the star was able to fit the predictions of the simulation, the uranium and thorium would have to fit under the expected values of the star. To do this, the simulation used to model the nucleosynthesis, which included the (n,f) rates, was used. The data was then put through chi-squared fitting for elements between Z=30 and 82, which are elements that are produced by the i-process. This compares these isotopes in both the simulation and from HE 0338-3945. From here, the cycle number with the lowest chi-squared value was selected as it would have the most similar i-process abundance pattern compared to HE 0338-3945. This abundance pattern was found when the simulated abundance was diluted with the solar abundance and the factor for the dilution was recorded. Once an ideal cycle was picked, it was used as the staring parameters and the simulation was run again, but for 10 Gyrs (10^{10} yrs) and

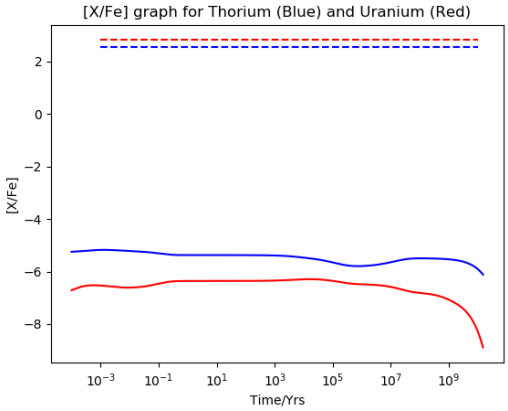

(a) [X/Fe] graph at temperature 1.75×10^8 K

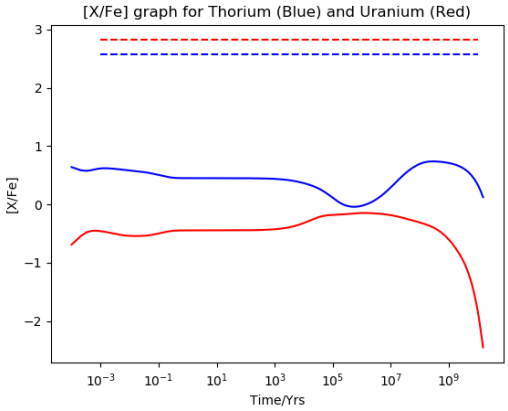

(b) [X/Fe] graph at temperature 2.00×10^8 K

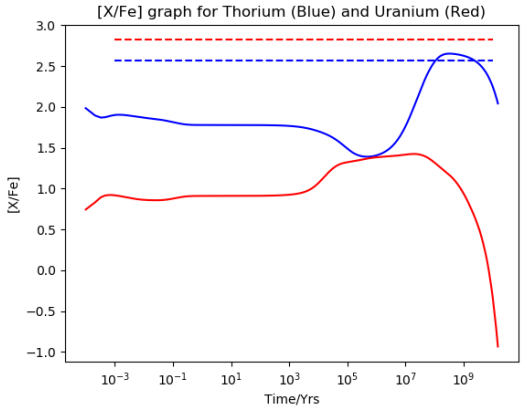

(c) [X/Fe] graph at temperature 2.25×10^8 K

Figure 4.1: Decaying [X/Fe] graphs for thorium and uranium for different temperatures. The temperature as the simulation decays is 1.00×10^7 K. Thorium is represented by the blue line and uranium by the red line. The dotted lines represent the values of thorium and uranium for the star HE 0338-3945 and the full line represents the paths as the elements decay.

at a lower temperature of 1.00×10^7 K. The increase in time meant that the unstable isotopes underwent decay as their half-lives had been reached, returning back to stability. The decrease in temperature stopped all i-process production, meaning the trans-lead isotopes created from the i-process would slowly reduce in number as they decayed. Once an abundance pattern was created, the thorium and uranium isotopes were diluted with the solar abundance by using the dilution factor found previously. These diluted elements were then compared to what is observed in HE 0338-3945. The whole procedure was repeated for three temperatures, 1.75×10^8 K, 2.00×10^8 K and 2.25×10^8 K runs.

The three graphs in figure 4.1 show [U/Fe] and [Th/Fe] as a function of time. This

abundance has been diluted with the solar abundances to more accurately portray a star with i-process materials. The change in time is over the span of 10 Gyrs and the system is set to a temperature of 1.00×10^8 K. At this temperature, i-process production has stopped and all unstable isotopes will decay back to stability, including the trans-lead isotopes. In figure 4.1a, with an initial temperature of 1.75×10^8 K, neither the thorium or uranium abundances reach the upper limits in HE 0338-3945 and is therefore a good representation for the star. The reason for this is that at this temperature, the star does not produce a significant amount of trans-lead isotopes, and so the decay of these isotopes reduces the abundances further. If the thorium or uranium abundances exceeded the upper limits of the star, then the simulation at that temperature would not be possible. Figure 4.1b shows the case when the temperature of the initial production is 2.00×10^8 K. This graph, much like the previous graph, does not produce significant thorium and uranium to reach the abundances of HE 0338-3945. However, we can see some key features of the abundances that are not obviously produced in the 1.75×10^8 K case. One of these features is detected at roughly 10^5 yrs, where ^{230}Th has reached its half-life and the overall abundance of thorium has reduced due to this decay. We can also see that at 10^7 yrs, the thorium abundance increases, due to the α decay of ^{236}U, which decays into ^{232}Th. Around 10^{10} yrs, we see that both thorium and uranium reduce significantly, as the time is longer than even the longest lived of those isotopes. Finally, we have figure 4.1c, which shows the case of a production temperature of 2.25×10^8 K. This graph has an overall higher abundance for both thorium and uranium compared to the previous two graphs. We can also see similar features in the evolution in Th & U as seen in figure 4.1b, but more clearly defined. There is also a more prominent increase in the abundance of uranium at 10^4 yrs. This feature is caused by ^{239}Pu, which has a half-life in this time frame and decays into ^{235}U, producing more uranium. The increase of thorium, due to the production of ^{232}Th as ^{236}U decays, has caused the abundance to exceed the abundance of thorium suggested by Jonsell et al. (2006). This means that the star from Jonsell et al. (2006) cannot be within this time period, as the thorium exceeds the limit for HE 0338-3945. In all runs shown in figure 4.1, the uranium abundance never reaches the upper limits determined by Jonsell et al. (2006).

Choplin et al. (2022) compared their results to their own star, RAVEJ094921.8 161722,

which showed that the thorium enrichment could be explained via the i-process without the need for other pollutants. These results line up with our own work and the comparisons with HE 0338-3945. As previously stated, the work done by Choplin et al. (2022) did not include the neutron induced fission reactions, which hamper the production of the upper section of the nuclide chart, especially as the test runs for a longer time. Were the reactions to be introduced we may see a slight change to their results.

5. Conclusion

The i-process has been successful in explaining the observed properties of certain stars. However, we are only just beginning to understand how the process works, and what isotopes it can produce. Most work has focused on the elements up to Pb, and little is known about the upper sections of the nuclide chart in regards to the i-process. One reason for this is that it is very difficult to detect spectroscopic lines of very heavy elements like uranium. However, it is not impossible and future abundance measurements may help us understand the i-process better. In this thesis I explored the potential for trans-lead isotopes being produced by the i-process. In order to properly model trans-Pb nucleosynthesis, we need to include the reactions for neutron-induced fission of heavy nuclei. The inclusion of the (n,f) rates for the trans-lead isotopes presented problems. Fission can split the nucleus into a range of products, which is difficult to deal with in our nucleosynthesis code. I therefore chose to approximate this by splitting the products into just two daughter nuclei. Many of the isotopes near the top of the nuclide chart were also not included in the (n,f) reactions, as these isotopes would not have been produced in significant amounts. The introduction of (n,f) rates reduces the abundance of trans-lead isotopes, as the fission takes place. The abundances of low mass isotopes increases slightly due to the daughter nuclei from the trans-lead isotopes, but not significantly. As for the results of the simulation without the (n,f) rates, we see that temperature change can effect the production of trans-lead isotopes, and the increase in temperature also speeds up the reactions. Without including (n,f) rates, substantial amounts of Th, U and others are produced. This decreased with the introduction of the (n,f) rates, as the trans-lead isotopes underwent fission.

Abundance measurements for trans-Pb elements are very rare. Only one star was discussed, HE 0338-3945, which has a heavy element pattern matching the i-process, has upper limits on the detection of thorium and uranium. These isotopes give a good indication as to the overall production of trans-lead isotopes. With the upper limits established, the simulation

does produce abundance patterns within the boundaries. However, with the changes in temperature, the thorium limit for HE 0338-3945 can be exceeded, specifically for a temperature of 2.25×10^8 K and only after a period of approximately 1×10^8 Yrs. This at least rules out 2.25×10^8 K as a possibility for temperature of HE 0338-3945.

There are several ways in which this work could be improved. The model for the neutron-induced fission was simplified. This was done by limiting the fission of a single isotope to only 2 fixed products. In reality, fission reactions have a distribution of products, can have more than 2 products and can also produce neutrons in addition to the daughter nuclei. Implementing these distributions into the simulation would more accurately display the lower sections of the nuclide chart. However, the emphasis of the thesis was looking at the trans-lead isotopes, and so the implementation of the distributions was not necessary. This is because the destruction of the heavy nuclei were key, and there would not be enough time for the recycling of material, unlike the r-process. Another improvement that could be implemented would be the inclusion of more stars to compare the results to, and therefore see if the thesis model fits within their abundance patterns. Only one star was compared to in this thesis, as it showed clear values for thorium and uranium, but other stars, like the one used in Choplin et al. (2022) could be used as well. We know we can reproduce the i-process patterns in several stars, but by using the simulation, it would be possible to predict what thorium and uranium abundances would be expected for others. This would give observers justification to apply for time in large telescopes, which is difficult to acquire.

The thesis went down one of several paths that could be used to simulate the production of trans-lead isotopes in a star. I have assumed an initial solar-scaled abundance distribution in these simulations, but other possibilities should be looked at. For example, it could be a viable method to start the simulation with an s-process abundance pattern, such as one found in a very late thermal pulse star, which would then undergo a proton ingestion. This would distribute heavier isotopes throughout the stable section of the nuclide chart, potentially making the production of trans-lead isotopes easier. Another, similar, method would be to have a star with a large initial abundance of lead. This seems logical as lead is the largest stable isotope and therefore would only need a nudge with the i-process to produce trans-lead

isotopes. The initial s-process method would also produce a build-up of lead, so the two methods could be the same.

A one-zone model takes one parameter from the overall stellar system to change, and keeps other parameters the same. A 1-D model changes all parameters involved, but does not look at the position in which the simulation takes place, but rather looks at how all parameters change within the model. It would be a good idea to compare the model from this thesis with the 1-D RAWD model calculated by Denissenkov et al. (2019), to see how the two line up with each other, if the 1-D model increases or decreases the production of trans-lead isotopes and if the trans-lead abundances are reasonable.

Bibliography

Asplund M., Lambert D. L., Kipper T., Pollacco D., Shetrone M. D., 1999, Astronomy and Astrophysics, 343, 507

Bisterzo S., Gallino R., Straniero O., Cristallo S., Käppeler F., 2012, Monthly Notices of the Royal Astronomical Society, 422, 849

Blake J. B., Schramm D. N., 1975, The Astrophysical Journal, 209, 615

Blake J. B., Schramm D. N., 1976, The Astrophysical Journal, 209, 846

Burbidge E. M., Burbidge G. R., Fowler W. A., Hoyle F., 1957, Reviews of Modern Physics, 29, 547

Busso M., Gallino R., Wasserburg G. J., 1999, Annual Review of Astronomy and Astrophysics, 37, 239

Cassisi S., Iben, Jr. I., Tornambe A., 1998, The Astrophysical Journal, 496, 376

Choplin A., Siess L., Goriely S., 2021, Astronomy and Astrophysics, 648

Choplin A., Goriely S., Siess L., 2022, Astronomy and Astrophysics, 667

Clarkson O., Herwig F., Pignatari M., 2018, Monthly Notices of the Royal Astronomical Society: Letters, 474, L37

Côté B., Denissenkov P., Herwig F., Ruiter A. J., Ritter C., Pignatari M., Belczynski K., 2018, The Astrophysical Journal, 854, 105

Cowan J. J., Rose W. K., 1977, The Astrophysical Journal, 212, 149

Cyburt R. H., et al., 2010, Astrophysical Journal, Supplement Series, 189, 240

Dardelet L., et al., 2018. p. 145

Denissenkov P. A., Herwig F., Battino U., Ritter C., Pignatari M., Jones S., Paxton B., 2017, The Astrophysical Journal, 834, L10

Denissenkov P. A., Herwig F., Woodward P., Andrassy R., Pignatari M., Jones S., 2019, Monthly Notices of the Royal Astronomical Society, 488, 4258

Gull M., et al., 2018, The Astrophysical Journal, 862, 174

Hampel M., 2015, Master's thesis, Rheinische Friedrich-Wilhelms-Universität Bonn

Hampel M., Stancliffe R. J., Lugaro M., Meyer B. S., 2016, The Astrophysical Journal, 831, 171

Hampel M., Karakas A. I., Stancliffe R. J., Meyer B. S., Lugaro M., 2019, Astrophysical Journal

Herwig F., et al., 2008, Nucleosynthesis simulations for a wide range of nuclear production sites from NuGrid, doi:10.48550

Herwig F., Pignatari M., Woodward P. R., Porter D. H., Rockefeller G., Fryer C. L., Bennett M., Hirschi R., 2011, Astrophysical Journal, 727

Jones S., Ritter C., Herwig F., Fryer C., Pignatari M., Bertolli M. G., Paxton B., 2016, Monthly Notices of the Royal Astronomical Society, 455, 3848

Jonsell K., Barklem P. S., Gustafsson B., Christlieb N., Hill V., Beers T. C., Holmberg J., 2006, Astronomy and Astrophysics, 451, 651

Malaney R. A., 1986, Monthly Notices of the Royal Astronomical Society, 223, 683

Panov I. V., Korneev I. Y., Rauscher T., Martínez-Pinedo G., Kelić-Heil A., Zinner N. T., Thielemann F.-K., 2010, Astronomy and Astrophysics, 513, A61

A. Appendix

A.1 Neutron Fission Tables

Isotope	(n,g) rate (s^{-1})	(n,f) rate (s^{-1})	ratio	Isotope	(n,g) rate (s^{-1})	(n,f) rate (s^{-1})	ratio
^{220}Th	6.590e+07	2.445e+05	3.711e-03	^{248}Th	1.703e+06	4.497e-08	2.641e-14
^{221}Th	1.828e+07	2.617e+08	1.432e+01	^{249}Th	1.152e+07	9.239e-03	8.017e-10
^{222}Th	1.002e+08	4.267e+05	4.259e-03	^{250}Th	1.599e+06	6.712e-08	4.197e-14
^{223}Th	1.400e+08	6.955e+07	4.968e-01	^{251}Th	6.342e+06	1.421e-02	2.240e-09
^{224}Th	9.623e+07	1.307e+06	1.358e-02	^{252}Th	2.929e+06	2.740e-07	9.354e-14
^{225}Th	4.626e+07	2.097e+08	4.532e+00	^{229}Pa	3.416e+03	2.553e+08	7.473e+04
^{226}Th	8.721e+07	4.407e+03	5.054e-05	^{230}Pa	2.528e+05	3.161e+08	1.250e+03
^{227}Th	9.242e+07	1.592e+08	1.722e+00	^{231}Pa	1.658e+08	2.392e+05	1.443e-03
^{228}Th	6.709e+07	8.614e+02	1.284e-05	^{232}Pa	3.121e+08	4.116e+08	1.319e+00
^{229}Th	9.377e+07	1.155e+08	1.232e+00	^{233}Pa	1.355e+08	1.076e+05	7.946e-04
^{230}Th	4.999e+07	6.765e+04	1.353e-03	^{234}Pa	2.306e+08	4.953e+07	2.148e-01
^{231}Th	8.097e+07	1.195e+08	1.476e+00	^{235}Pa	8.117e+07	1.876e+02	2.311e-06
^{232}Th	3.279e+07	4.151e+02	1.266e-05	^{236}Pa	2.188e+08	1.603e+06	7.328e-03
^{233}Th	5.934e+07	1.709e+07	2.880e-01	^{237}Pa	4.353e+07	4.565e-02	1.049e-09
^{234}Th	1.779e+07	4.479e-01	2.518e-08	^{238}Pa	2.135e+08	2.880e+02	1.349e-06
^{235}Th	6.760e+07	4.826e+03	7.140e-05	^{239}Pa	2.550e+08	1.186e-01	4.649e-10
^{236}Th	3.138e+07	9.437e-01	3.007e-08	^{240}Pa	6.242e+08	2.306e+02	3.694e-07
^{237}Th	3.564e+07	9.837e+01	2.760e-06	^{241}Pa	2.277e+08	2.320e-03	1.019e-11
^{238}Th	1.333e+07	2.864e-03	2.148e-10	^{242}Pa	4.924e+08	7.926e+00	1.610e-08
^{239}Th	7.637e+07	6.076e+01	7.955e-07	^{243}Pa	2.609e+08	1.438e-04	5.512e-13
^{240}Th	1.187e+07	3.077e-05	2.593e-12	^{244}Pa	1.723e+08	2.628e-01	1.525e-09
^{241}Th	4.731e+07	1.374e-01	2.904e-09	^{245}Pa	2.646e+08	1.775e-05	6.710e-14
^{242}Th	1.251e+07	4.207e-08	3.363e-15	^{246}Pa	1.483e+08	4.220e-02	2.846e-10
^{243}Th	2.182e+07	1.115e-03	5.109e-11	^{247}Pa	2.198e+08	2.738e-04	1.246e-12
^{244}Th	9.493e+06	3.566e-08	3.756e-15	^{248}Pa	1.390e+08	2.136e-01	1.536e-09
^{245}Th	1.259e+07	1.054e-04	8.374e-12	^{249}Pa	1.546e+08	3.839e-04	2.484e-12
^{246}Th	5.638e+06	1.978e-08	3.507e-15	^{250}Pa	8.309e+07	8.239e+00	9.915e-08
^{247}Th	1.024e+07	4.199e-04	4.100e-11	^{251}Pa	1.272e+08	2.008e-02	1.578e-10

Isotope	(n,g) rate (s^{-1})	(n,f) rate (s^{-1})	ratio	Isotope	(n,g) rate (s^{-1})	(n,f) rate (s^{-1})	ratio
^{252}Pa	4.727e+07	2.910e+01	6.156e-07	^{236}Np	7.817e+07	3.655e+08	4.676e+00
^{230}U	1.957e+06	3.435e+08	1.756e+02	^{237}Np	1.993e+08	1.769e+06	8.873e-03
^{231}U	3.107e+06	3.451e+08	1.111e+02	^{238}Np	1.122e+07	5.085e+08	4.534e+01
^{232}U	6.436e+07	2.081e+08	3.233e+00	^{239}Np	2.126e+08	4.359e+06	2.050e-02
^{233}U	8.343e+06	3.791e+08	4.544e+01	^{240}Np	3.914e+08	4.987e+06	1.274e-02
^{234}U	7.536e+07	1.719e+06	2.281e-02	^{241}Np	2.264e+08	6.929e+02	3.061e-06
^{235}U	1.346e+07	4.669e+08	3.468e+01	^{242}Np	1.760e+08	6.773e+03	3.848e-05
^{236}U	5.228e+07	1.062e+05	2.031e-03	^{243}Np	3.521e+08	3.092e-01	8.782e-10
^{237}U	5.840e+07	1.231e+08	2.108e+00	^{244}Np	5.114e+08	5.574e+02	1.090e-06
^{238}U	3.410e+07	1.626e+03	4.767e-05	^{245}Np	4.005e+08	2.584e-01	6.453e-10
^{239}U	8.819e+07	2.694e+07	3.055e-01	^{246}Np	4.477e+08	1.642e+02	3.667e-07
^{240}U	2.489e+07	1.798e+01	7.224e-07	^{247}Np	4.676e+08	9.708e+00	2.076e-08
^{241}U	7.726e+07	2.034e+04	2.633e-04	^{248}Np	2.425e+08	5.423e+01	2.236e-07
^{242}U	3.462e+07	2.286e+00	6.604e-08	^{249}Np	4.110e+08	3.145e+01	7.651e-08
^{243}U	8.611e+07	9.099e+02	1.057e-05	^{250}Np	1.716e+08	1.108e+03	6.457e-06
^{244}U	2.690e+07	1.313e-01	4.879e-09	^{251}Np	2.216e+08	8.238e+02	3.718e-06
^{245}U	5.082e+07	8.462e+01	1.665e-06	^{252}Np	2.359e+08	3.545e+06	1.503e-02
^{246}U	1.693e+07	5.411e-01	3.196e-08	^{234}Pu	4.193e+06	4.685e+08	1.117e+02
^{247}U	2.351e+07	2.228e+01	9.475e-07	^{235}Pu	1.906e+06	5.028e+08	2.638e+02
^{248}U	1.144e+07	8.789e-01	7.682e-08	^{236}Pu	1.082e+07	4.595e+08	4.246e+01
^{249}U	1.721e+07	3.495e+02	2.031e-05	^{237}Pu	3.618e+06	5.649e+08	1.561e+02
^{250}U	7.295e+06	1.490e+01	2.042e-06	^{238}Pu	1.157e+08	3.353e+07	2.897e-01
^{251}U	2.696e+07	7.060e+03	2.619e-04	^{239}Pu	8.065e+06	5.553e+08	6.886e+01
^{252}U	4.529e+06	1.469e+01	3.242e-06	^{240}Pu	7.458e+07	4.441e+06	5.955e-02
^{232}Np	3.003e+06	3.899e+08	1.298e+02	^{241}Pu	6.653e+06	7.097e+08	1.067e+02
^{233}Np	1.076e+07	3.977e+08	3.695e+01	^{242}Pu	4.907e+07	3.540e+06	7.214e-02
^{234}Np	2.821e+08	1.430e+09	5.069e+00	^{243}Pu	9.446e+06	6.918e+08	7.324e+01
^{235}Np	1.173e+08	2.179e+08	1.858e+00	^{244}Pu	2.663e+07	2.204e+06	8.276e-02

Isotope	(n,g) rate (s^{-1})	(n,f) rate (s^{-1})	ratio	Isotope	(n,g) rate (s^{-1})	(n,f) rate (s^{-1})	ratio
^{245}Pu	5.649e+07	2.213e+08	3.918e+00	^{244}Cm	1.139e+08	1.873e+07	1.645e-01
^{246}Pu	5.025e+07	4.095e+06	8.149e-02	^{245}Cm	2.689e+06	9.397e+08	3.494e+02
^{247}Pu	6.196e+07	4.848e+03	7.823e-05	^{246}Cm	3.789e+07	2.689e+07	7.098e-01
^{248}Pu	4.648e+07	1.300e+02	2.797e-06	^{247}Cm	2.593e+07	2.432e+08	9.380e+00
^{249}Pu	3.580e+07	1.705e+04	4.764e-04	^{248}Cm	3.439e+07	4.980e+06	1.448e-01
^{250}Pu	2.804e+07	5.679e+03	2.025e-04	^{249}Cm	9.945e+06	6.222e+08	6.257e+01
^{251}Pu	3.616e+07	6.928e+05	1.916e-02	^{250}Cm	3.376e+07	8.920e+04	2.642e-03
^{252}Pu	8.856e+06	6.238e+04	7.044e-03	^{251}Cm	2.387e+08	9.380e+05	3.930e-03
^{238}Am	1.815e+08	8.724e+08	4.807e+00	^{252}Cm	7.623e+07	4.551e+04	5.971e-04
^{239}Am	2.431e+08	4.142e+07	1.704e-01	^{243}Bk	3.994e+08	2.137e+07	5.349e-02
^{240}Am	2.978e+07	5.983e+08	2.009e+01	^{244}Bk	4.813e+08	1.263e+09	2.624e+00
^{241}Am	2.243e+08	1.449e+06	6.459e-03	^{245}Bk	3.459e+08	9.073e+06	2.623e-02
^{242}Am	3.975e+07	6.181e+08	1.555e+01	^{246}Bk	1.072e+09	1.013e+09	9.448e-01
^{243}Am	2.008e+08	2.046e+06	1.019e-02	^{247}Bk	2.172e+08	3.145e+06	1.448e-02
^{244}Am	3.274e+08	1.088e+08	3.322e-01	^{248}Bk	2.366e+08	3.431e+08	1.450e+00
^{245}Am	1.616e+08	2.588e+07	1.601e-01	^{249}Bk	1.951e+08	2.560e+05	1.312e-03
^{246}Am	2.376e+08	2.347e+08	9.876e-01	^{250}Bk	2.278e+08	9.495e+07	4.167e-01
^{247}Am	2.749e+08	2.390e+00	8.692e-09	^{251}Bk	1.410e+08	1.069e+01	7.577e-08
^{248}Am	3.891e+08	1.898e+04	4.877e-05	^{252}Bk	5.415e+08	1.895e+03	3.499e-06
^{249}Am	2.653e+08	5.355e+02	2.018e-06	^{245}Cf	3.302e+08	1.444e+08	4.373e-01
^{250}Am	3.152e+08	6.943e+04	2.203e-04	^{246}Cf	1.860e+08	7.668e+05	4.123e-03
^{251}Am	2.315e+08	7.226e+02	3.121e-06	^{247}Cf	3.366e+08	2.616e+06	7.770e-03
^{252}Am	2.871e+08	3.546e+05	1.235e-03	^{248}Cf	1.621e+08	8.591e+03	5.300e-05
^{240}Cm	1.608e+08	5.822e+07	3.620e-01	^{249}Cf	4.555e+06	7.504e+08	1.647e+02
^{241}Cm	5.386e+07	8.024e+08	1.490e+01	^{250}Cf	6.467e+07	3.402e+06	5.260e-02
^{242}Cm	1.177e+08	3.808e+06	3.236e-02	^{251}Cf	3.851e+05	8.887e+08	2.308e+03
^{243}Cm	1.100e+07	6.850e+08	6.226e+01	^{252}Cf	6.464e+06	2.293e+08	3.548e+01

Trans-Lead Isotope	Daughter Nuclei 1	Daughter Nuclei 2
^{229}Th	^{138}Xe	^{92}Sr
^{230}Th	^{139}Cs	^{92}Sr
^{231}Th	^{139}Cs	^{93}Sr
^{232}Th	^{140}Cs	^{93}Sr
^{233}Th	^{140}Cs	^{94}Sr
^{234}Th	^{141}Ba	^{94}Sr
^{235}Th	^{142}Ba	^{94}Sr
^{236}Th	^{142}Ba	^{95}Y
^{237}Th	^{143}Ba	^{95}Y
^{238}Th	^{143}Ba	^{96}Y
^{239}Th	^{144}La	^{96}Y
^{240}Th	^{145}La	^{96}Y
^{241}Th	^{145}La	^{97}Zr
^{242}Th	^{146}Ce	^{97}Zr
^{233}Pa	^{140}Cs	^{94}Sr
^{334}Pa	^{141}Ba	^{94}Sr
^{235}Pa	^{142}Ba	^{94}Sr
^{236}Pa	^{142}Ba	^{95}Y
^{237}Pa	^{143}Ba	^{95}Y
^{238}Pa	^{143}Ba	^{96}Y
^{239}Pa	^{144}La	^{96}Y
^{240}Pa	^{145}La	^{96}Y
^{241}Pa	^{145}La	^{97}Zr

Trans-Lead Isotope	Daughter Nuclei 1	Daughter Nuclei 2
^{242}Pa	^{146}Ce	^{97}Zr
^{243}Pa	^{146}Ce	^{98}Zr
^{244}Pa	^{147}Ce	^{98}Zr
^{245}Pa	^{148}Ce	^{98}Zr
^{246}Pa	^{148}Ce	^{99}Nb
^{247}Pa	^{149}Ce	^{99}Nb
^{235}U	^{142}Ba	^{94}Sr
^{236}U	^{142}Ba	^{95}Y
^{237}U	^{143}Ba	^{95}Y
^{238}U	^{143}Ba	^{96}Y
^{239}U	^{144}La	^{96}Y
^{240}U	^{145}La	^{96}Y
^{241}U	^{145}La	^{97}Zr
^{242}U	^{146}Ce	^{97}Zr
^{243}U	^{146}Ce	^{98}Zr
^{244}U	^{147}Ce	^{98}Zr
^{245}U	^{148}Ce	^{98}Zr
^{246}U	^{148}Ce	^{99}Nb
^{247}U	^{149}Pr	^{99}Nb
^{239}Np	^{144}La	^{96}Y
^{240}Np	^{145}La	^{96}Y
^{241}Np	^{145}La	^{97}Zr
^{242}Np	^{146}Ce	^{97}Zr

Table A.4: List of trans-lead isotopes with included (n,f) rates, along with daughter nuclei produced. Daughter nuclei have been decayed so that they decay onto the i-process material. Isotopes ^{229}Th - ^{242}Np.

Trans-Lead Isotope	Daughter Nuclei 1	Daughter Nuclei 2
^{243}Np	^{146}Ce	^{98}Zr
^{244}Np	^{147}Ce	^{98}Zr
^{245}Np	^{148}Ce	^{98}Zr
^{246}Np	^{148}Ce	^{99}Nb
^{247}Np	^{149}Pr	^{99}Nb
^{248}Np	^{149}Pr	^{100}Nb
^{249}Np	^{150}Pr	^{100}Nb
^{250}Np	^{151}Pr	^{100}Mo
^{251}Np	^{151}Pr	^{101}Mo
^{241}Pu	^{145}La	^{97}Zr
^{242}Pu	^{146}Ce	^{97}Zr
^{243}Pu	^{146}Ce	^{98}Zr
^{244}Pu	^{147}Ce	^{98}Zr
^{245}Pu	^{148}Ce	^{98}Zr
^{246}Pu	^{148}Ce	^{99}Nb
^{247}Pu	^{149}Pr	^{99}Nb
^{248}Pu	^{149}Pr	^{100}Nb
^{249}Pu	^{150}Pr	^{100}Nb
^{250}Pu	^{151}Pr	^{100}Mo
^{251}Pu	^{151}Pr	^{101}Mo
^{252}Pu	^{152}Nd	^{101}Mo
^{243}Am	^{146}Ce	^{98}Zr
^{244}Am	^{147}Ce	^{98}Zr

Trans-Lead Isotope	Daughter Nuclei 1	Daughter Nuclei 2
^{245}Am	^{148}Ce	^{98}Zr
^{246}Am	^{148}Ce	^{99}Nb
^{247}Am	^{149}Pr	^{99}Nb
^{248}Am	^{149}Pr	^{100}Nb
^{249}Am	^{150}Pr	^{100}Nb
^{250}Am	^{151}Pr	^{100}Mo
^{251}Am	^{151}Pr	^{101}Mo
^{252}Am	^{152}Nd	^{101}Mo
^{245}Cm	^{148}Ce	^{98}Zr
^{246}Cm	^{148}Ce	^{99}Nb
^{247}Cm	^{149}Pr	^{99}Nb
^{248}Cm	^{149}Pr	^{100}Nb
^{249}Cm	^{150}Pr	^{100}Nb
^{250}Cm	^{151}Pr	^{100}Mo
^{251}Cm	^{151}Pr	^{101}Mo
^{252}Cm	^{152}Nd	^{101}Mo
^{249}Bk	^{150}Pr	^{100}Nb
^{250}Bk	^{151}Pr	^{100}Mo
^{251}Bk	^{151}Pr	^{101}Mo
^{252}Bk	^{152}Nd	^{101}Mo
^{251}Cf	^{151}Pr	^{101}Mo
^{252}Cf	^{152}Nd	^{101}Mo

Table A.5: List of trans-lead isotopes with included (n,f) rates, along with daughter nuclei produced. Daughter nuclei have been decayed so that they decay onto the i-process material. Isotopes ^{243}Np - ^{252}Cf.